



UPPSALA
UNIVERSITET

Department of Physics and Astronomy

November 2019

Master's Thesis Astrophysics

30 ECTS

Conditions for detecting Population III galaxies with next-generation telescopes

Emma Fransson

Supervisor: *Erik Zackrisson*
Subject reader: *Kjell Olofsson*
Examiner: *Andreas Korn*



Populärvetenskaplig sammanfattning

Hur gick det till när vårt universum övergick från att vara en mörk plats enbart uppbyggt av de enkla grundämnena som bildats efter big bang, till att fyllas av de första, starkt lysande stjärnorna? Hittills har man inte kunnat se så långt bak i universums historia, men man har med hjälp av teori och simuleringar skapat sig en bild över hur det kan ha sett ut när gas drog sig samman tills temperaturen och trycket blev tillräckligt högt för att materia skulle kunna tändas i de allra första stjärnorna. Detta tros ha hänt inuti väldigt massiva halos av mörk materia som med sin gravitation underlättade för den ordinära materia att dra sig samman.

Det som gör dessa första stjärnor så unika är att de enbart består av de beståndsdelar som fanns att tillgå efter big bang; det vill säga väte, helium och små spår av litium. Tyngre grundämnena bildas när massiva stjärnor genomgår en supernova, något som dessa första stjärnor kunde bidra med först när de brunnit ut. Denna sammansättning gjorde att de allra första stjärnorna var mer massiva än de som vi observerar idag. Detta beror på att när gas drar ihop sig måste den kylas för att det termiska trycket som ökar vid kontraktion inte ska bli för stort och motverka gasens kollaps till en stjärna. Kylning sker genom att molekyler och atomer absorberar energi genom kollisioner och sedan avger denna energi genom att stråla iväg ljus. Denna process är mer effektiv för tyngre grundämnena jämfört med väte och helium, så kylning av ett icke förorenat gasmoln i universums ungdom kyls reellt långsamt. Detta gör att temperatur och tryck ges tid att jämnas ut genom gasmolnet, något som förhindrar att molnet fragmenteras i alltför stor grad och då istället bildar mindre stjärnor. De första stjärnorna var alltså väldigt massiva, något som kan översättas till kortare livstider då massiva stjärnor, lite kontraintuitivt, snabbare använder upp sitt bränsle. Att vi ska kunna observera dessa första stjärnor en och en har hittills inte varit möjligt, då vi måste blicka väldigt långt bak i tiden, för långt bak för att ljuset från en isolerad stjärna skulle vara tillräckligt för att det ska nå våra nuvarande teleskop. Istället riktas blicken mot samlingar av dessa första stjärnor, mot galaxer bestående av denna oförorenade generation av stjärnor. Här används modeller över hur dessa galaxer kan ha sett ut för att försöka beräkna hur starkt de lyst och om detta ljus är tillräckligt för att nå detektorerna hos de kraftfulla teleskop som idag står i startgroparna, snart redo att inleda sina observationer. Det finns även en joker med i leken som kan underlätta i jakten på ljuset från universums vagg, nämligen gravitationslinserna; universums egna förstoringsglas. När ljus passerar väldigt massiva objekt i rymden, påverkas det och under rätt förutsättningar kan resul-

tatet bli att vi mottar en ökad ljusmängd från den avlägsna källan. Denna process kan göra att ljus som egentligen ligger under gränsen för detektion hos teleskopen får en knuff in i den observerbara regimen. Modellerna över de första galaxernas utstrålade ljus i kombination med fysiken bakom denna förstoring och sannolikheterna för att ett avlägset objekt ska hamna rätt relativt linsen kombineras i denna rapport. Detta för att få fram i vilken utsträckning dessa mycket avlägsna galaxer måste ha bildats för att de kommande teleskopen ska kunna observera dem. Förutsatt att den nuvarande bilden över universums historia och de fysikaliska processer som format den inte är för långt från sanningen finns det goda chanser att kunna detektera dessa galaxer med de välplanerade teleskopen som inom kort kommer att skickas upp i omloppsbanan och börja förse oss med information.

Acknowledgments

My deep gratitude goes my supervisor Erik Zackrisson for his great patience and enormous flexibility during this project.

Contents

1	Introduction	6
2	Population III stars and galaxies	8
2.1	Formation of population III stars	8
2.1.1	Cooling	8
2.1.2	Dark matter halos	10
2.1.3	Formation of population III stars at different redshifts	11
2.1.4	Did population III stars contribute to the reionization of the universe?	11
2.2	Mass distribution	12
2.3	Delayed formation	13
2.3.1	Lyman Werner radiation	13
2.3.2	Baryonic streaming motion	13
2.4	Population III galaxies	14
2.5	Predicted number densities of Population III galaxies	14
2.5.1	M. Stiavelli and M. Trenti 2010	15
2.5.2	K. Inayoshi et al 2018	15
2.6	Characteristics for detection	16
2.6.1	Lyman alpha	17
2.6.2	He II 1640 Å	17
3	Gravitational lensing	18
3.1	Geometry	18
3.1.1	Caustic and critical curves	20
3.2	Magnification	20
4	Next generation telescopes	22
4.1	WFIRST	22
4.2	JWST	22
4.3	Euclid	23
4.4	Detection limits	23
5	Method/Background	24
5.1	Yggdrasil spectral synthesis model	24

5.1.1	PopIII.1	25
5.1.2	PopIII.2	25
5.1.3	PopIII Kroupa	25
5.1.4	Parameters	25
5.2	Magnification data	26
5.2.1	Inter- and extrapolating data	26
5.3	Equivalent width of He II	28
5.4	Estimating the detectability of Pop III galaxies	30
6	Results	32
6.1	Photometry	32
6.1.1	Formation rate of population III galaxies as a function of source redshift	32
6.1.2	Covering factor 1 and 0.5	32
6.1.3	Star formation history over 10 million years compared to an instantaneous star burst	33
6.2	Spectroscopy	35
6.2.1	HeII 1640 Å flux	35
6.2.2	Number densities required for detection of He II emission line	38
6.3	Comparing detectability	38
6.3.1	Photometry	43
6.3.2	Spectroscopy	43
7	Conclusions	52
7.1	Future outlook	52

1 Introduction

At some point, the universe transitioned from the so called dark ages into the still ongoing era of stellar formation. As the first stars ignited, they started radiating, giving off the very first light. The detection of this light is essential for gaining knowledge on the earlier state of our cosmos. All stars observed so far exhibit lines of heavier elements in their spectra; elements that in turn are the products of the violent deaths of previous, massive stars. Since the early state of the universe is predicted to contain only hydrogen, helium and some trace amounts of lithium (Ryan et al 2000), there must have been a first generation of stars that was formed from only this primordial material. These stars are called population III stars and they are predicted to have been the creators of the first heavier elements of the universe and then also provide the building blocks of the stars we observe today. The detection of population III stars is often referred to as one of the holy grails in astronomy due to the fact that in spite of the many predictions of their existence they still remain a mystery.

There exist different explanations for why these long sought-after stars have yet to be discovered. One suggestion is that they have accreted an atmosphere of enriched materials as the material of the universe evolved, masking their true pristine nature (A. Tanikawa et al. 2018). Another is that heavier elements formed in the interior of the star have found their way to the surface, making an imprint on the stellar spectra (L. Germany et al.). A more probable explanation is that the first stars were very massive, with the consequence that they only existed for a short period of time before they exhausted their fuel and turned supernova or collapsed directly into black holes. This is supported by the fact that no red dwarfs without metal lines in their spectra have so far been detected. These stars represent the low mass end of the stellar mass spectra and they have lifetimes exceeding the age of the universe many times over. This means that if low mass population III stars did form, they would still be here for us to detect today, but this does not appear to be the case.

The theory and lack of observations points towards the first stars being very massive and living short, violent lives. The question is; how can they be detected? In order to assess the prospects of detection, a model for their formation, evolution and radiation needs to be synthesized. The chances of detecting single population III stars with the available machinery of today does not appear possible (C. Rydberg et al. 2012) so the attention is instead shifted towards population III galaxies, whose integrated light provide a more promising candidate (E. Zackrisson et al. 2012).

The following work is concerned with obtaining minimum number densities and formation rates required for detection of population III galaxies. In order to achieve that, the luminosity and spectral behavior of these galaxies are needed, something that is provided by the spectral synthetic model Yggdrasil (E. Zackrisson et al. 2011). Searching for population II stars is also a matter of looking far back into time, operating at uncomfortably high redshifts. This means that the intrinsic luminosity of the objects of interest might not be sufficient and magnification by gravitational lensing needs to be incorporated in the calculations in order to push the received flux above the detection limits of the proposed telescopes.

There are a lot of uncertainties involved in trying to predict the radiation from the earliest stars. The high-redshift part of the universe is still unobserved, so the provided spectral features need to be based on simulations. Another unknown property is the mass distribution among population III stars. They are predicted to be characterized by higher masses compared to more modern stars, but the shape of the distribution is unclear. This motivates the use of, and comparison between, models with different initial mass functions.

If the existing models and their assumptions are not too far from the true nature of population III galaxies, a confirmed detection is not out of reach for planned telescope missions like the Wide Field InfraRed Survey (WFIRST) or the James Webb Space Telescope (JWST) that will launch within the next decade.

2 Population III stars and galaxies

2.1 Formation of population III stars

The circumstance which sets the formation of stars from primordial material apart from the stars forming from material containing metals is that their evolution can be modeled in a somewhat more straightforward way, especially regarding the mechanism for cooling. This is in a sense easier to set up for primordial stars since it is mainly concerned with atomic and molecular hydrogen, the simplest of all elements. Another restriction is the fact that there are no prior stars present that can influence the formation of at least the very first generation of population III stars (P.H. Bodenheimer 2011). For population III galaxies the case is different since they, as described below, depend on the radiation from nearby stellar populations to be able to form and also require that the halo produces more than just one star.

When modeling star formation at a later stage in the evolution of the universe and its contents, the simulations are often forced to be based on a row of simplifications in order for the data power to be sufficient. This is in a way already built in for population III stars since they emerge from a simpler universe (P.H. Bodenheimer 2011). With that said it is still no trivial task trying to understand the formation of these stars and their galaxies.

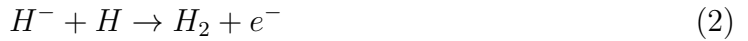
The current general model for star formation describes how gas collapses under its own gravity until the inner thermal pressure halts the process and hydrostatic equilibrium sets in. In order for collapse to be initiated the gas cloud needs to lose the counterforce of gravity, namely its thermal energy. This means that the gas needs to cool in order to be able to contract.

2.1.1 Cooling

The cooling mechanism is mainly due to radiative cooling, a process that is more efficient when heavier elements are present. The electrons in an atom get excited by absorbing energy through collisions and when they undergo de-excitation they emit photons that carry the energy out from the cloud, which then decreases in temperature. For a cloud of pristine material, the radiative cooling can only happen through helium and hydrogen, where the latter is the most important. Atomic hydrogen is important for the cooling process, especially at higher temperatures and larger masses, but it is molecular hydrogen, H_2 , that mainly contributes in lowering the temperature. It acts as the main

channel in halos of lower mass but it is also important in the later stage in the cooling of more massive halos.

A major issue with the cooling through H_2 is that it does not form in a straightforward reaction. The formation of molecular hydrogen in our present day takes place in the vicinity of dust grains that can act as absorbers of the excess energy that quickly needs to be released from the highly unstable protomolecule of H_2 (V. Pirronello et al. 1998). This is clearly not possible in a cloud of dust-free, primordial material. Direct attachment of the hydrogen atoms is not quantum mechanically allowed since it violates a forbidden transition. Another obstacle is that at the time of formation of the first stars, the universe was neutral and the fraction of electrons and hydrogen ions to neutral hydrogen was very small, slowing the formation of H_2 that took place through the following interactions (P.H. Bodenheimer 2011):



or



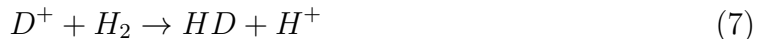
These reactions only produce a small amount of molecular hydrogen due to the low densities of its reactants. When the density reaches $n = 10^8 \text{cm}^{-3}$, a three-body reaction to produce H_2 becomes possible and the abundance of the molecule increases considerably.



In order to excite H_2 to the first level a temperature of 512 K is needed, so cooling of the cloud via H_2 can only be done down to approximately 200 K. At this temperature there still exists a considerable amount of particles with enough energy in the high

energy tail of the Maxwell velocity distribution to enable excitation of the molecular hydrogen (P.H. Bodenheimer 2011).

In mass sufficiently high temperatures, cooling through atomic hydrogen becomes important. Halos with masses $10^7 - 10^8 M_\odot$ reach temperatures of roughly $10^4 K$, which is enough to partially ionize the gas¹. This means that the fraction of free electrons goes up and this in turn provides more building blocks for the formation of molecular hydrogen. In the inner regions of the atomic cooling halos, the density of molecular hydrogen goes up, speeding up the cooling process. Due to the fact that the gas is ionized, another molecule can also form, namely hydrogen deuteride (HD), through the following reaction:



The ratio of D/H is small, $\sim 10^{-5}$, but the resulting formation of HD is still of great importance since it is a very efficient coolant, offering rotational transitions that has a higher spontaneous rate of occurrence compared to that of H_2 . In a mini halo, a halo with a mass of $\sim 10^6 M_\odot$, cooling through H_2 can, as mentioned above, lower the temperature to approximately 200 K but in a more massive, atomic cooling halo the HD molecule can lower the temperature as far as radiative cooling can; down to the temperature of the CMB background (J.L. Johnson 2011).

2.1.2 Dark matter halos

The formation of population III stars is believed to have started in dark matter halos of the early universe. These halos are the product of small inhomogeneities in the matter distribution of the early universe that grew larger with time. Overdense regions of mainly dark matter grew larger with encounters and mergers and provided gravitational potentials for the baryons to follow and finally settle as the main constituent of the halo core (P.H. Bodenheimer 2011). As the gas contracts, it is photoionized and photoheated and forms a pressure-supported system in the core of the dark matter halo. The halo grows, causing further pressure on the core, and increases its density. When the density goes up, the recombination rate in the core follows, increasing the neutral fraction of hydrogen. When the heating timescale exceeds the dynamical timescale a runaway collapse is initiated resulting in star formation (E. Visbal et al. 2017).

¹To note is that at $z > 16$, pristine halos in this range are predicted to be very rare due to enrichment from population II stars, so this is not applicable for higher z .

As mention above it is hydrogen in different shapes that provides the main channel for cooling a pristine cloud, where molecular hydrogen is the main coolant in low-mass halos and atomic hydrogen becomes important at the higher temperatures of more massive halos (M. Stiavelli & M. Trenti 2009).

2.1.3 Formation of population III stars at different redshifts

An investigation concerned with how different halo masses affected the formation of population III stars was conducted by Stiavelli and Trenti 2009 and their results can be summarized as follows. For low mass halos at very high redshifts around 60, it is enough with a mass of approximately $4 * 10^4 M_{\odot}$ for enabling cooling through molecular hydrogen. With lower redshifts, this mass increases but this is in turn balanced by the simultaneous increase in the abundances of these halos. This enables the formation rate of population III stars to continue to rise until the radiative feedback becomes important, around $z=35$, and the formation rate levels out at one star per $cMpc^3$ per unit redshift. High mass halos on the other hand, follow a different track. In the presence of molecular hydrogen these halos cool, initiate star formation and get enriched fast. This can be halted by radiative feedback, mainly provided by stars in the smaller halos. The formation rate of stars in these halos only exceed that of the smaller ones when Lyman Werner radiation efficiently suppress cooling by molecular hydrogen at a redshift of $z \approx 14$ (M. Stiavelli & M. Trenti 2009).

2.1.4 Did population III stars contribute to the reionization of the universe?

Surveys done by WMAP of the cosmic microwave background concludes a low optical depth for the reionization phase of the universe which suggests that this was an almost instantaneous process at around redshift ten. The question of which role that population III stars might have played in this still remains to be answered (M. Stiavelli & M. Trenti 2009).

If low-mass dark matter halos were the dominant channel for population III star formation, with one star forming in each halo, the number density of these stars would not have been sufficient to have a real impact on the ionization process. This is in spite of population III stars having at least one order of magnitude higher efficiency in producing ionizing radiation compared to the following generations. Not even with an escape fraction approaching unity could they have ionized a significant fraction of the hydrogen present in the universe. (M. Stiavelli & M. Trenti 2009).

A recent detection done by EDGES (the Experiment to Detect the Global Epoch of Reionization Structure) shows an absorption at the 21 cm neutral hydrogen line at $z \sim 17$, which is not compatible with the existing theories. With an amplitude of three times that expected from a Λ CDM cosmology this detection raises several questions. One explanation for the detection could be that there were a much stronger Lyman alpha field present at these high redshifts than currently believed. Lyman alpha photons can excite an hydrogen atom from its anti-parallel ground state to the P state. When the atom then de-excites it instead settles in the slightly more energetic parallel spin ground state with the result that a photon with lower energy is emitted. This process leaves an absorption feature in the spectra. The 21 cm detection could then be a sign of more substantial emissions by population III stars than previously believed, but it could also be a sign of previously unknown dark matter physics (A.T.P. Schauer et al. 2019).

2.2 Mass distribution

The initial mass function (IMF) of population III stars is predicted to be top-heavy, i.e pushed towards larger masses compared to the IMF of later generations of stars. The prediction that the first stars should have been very massive is one thing to make, but the detailed shape of the mass distribution is still highly uncertain. Initially it was proposed that the IMF of population III stars peaked at around $100M_{\odot}$ (M. Stiavelli & M. Trenti 2009) but a lower number around $10M_{\odot}$ has also been suggested (A. Stacy et al. 2010). The true value may very well reside somewhere in between or there might even have been two close star bursts with different peaks in mass (J.L. Johnson 2011).

The reason for why these stars are believed to be more massive than the current stellar population is due to the metal deficiency and its effect on the cooling mechanism. A metal enriched cloud can efficiently shed its thermal energy giving a contraction fast enough for fragmentation to occur, meaning that different overdense regions in the cloud form individual clumps of material. When no metals are present, the cooling is much slower and thermal pressure becomes important at an earlier state which slows the contraction before a large part of the fragmentation can take place. Temperature and pressure have time to equalize across the cloud resulting in larger structures that with time becomes large stars (P.H. Bodenheimer 2011).

2.3 Delayed formation

One possibility for making the detection of population III stars more accessible is if their formation can be delayed by some process. One such mechanism could be if pockets of pristine material can be preserved without pollution from nearby star evolution and that the initiation of star formation is suppressed. This is also a suggested possibility behind the formation of entire galaxies of population III stars, that form chronologically after the first galaxies.

2.3.1 Lyman Werner radiation

Lyman Werner (LW) radiation is ultraviolet radiation in the interval 11.2-13.6 eV, corresponding to an suitable energy range for absorption by molecular hydrogen. Since molecular hydrogen is a key ingredient for cooling primordial clouds, star formation in these can be inhibited if the formation of H_2 is initially inhibited. This can be achieved by LW radiation that photodissociates the molecules leading to suppression of star formation until cooling by atomic hydrogen becomes efficient, which happens at around 10^4 Kelvin. The LW photon flux required to suppress star formation significantly beyond the atomic cooling threshold is approximately $10^6 s^{-1} cm^{-2}$. At high redshifts, these fluxes are found near star forming galaxies (E. Visbal et al. 2017).

2.3.2 Baryonic streaming motion

Another mechanism for delaying star formation in the early universe is the streaming motions of baryons. Before baryons decouple from photons at $z=1100$, they were carried along with the photons which meant that they had a velocity relative to dark matter that only responds to gravity. These relative velocities are after recombination translated into baryonic streaming motions (BSM), a shock inducing force that can delay star formation by dissociate molecular hydrogen (K. Inayoshi et al. 2018, A. Fialkov et al. 2012). The shock is created when the BSM comes in against the movements of the dark matter halo itself, disrupting the material. Simulations show that the probability of being exposed for these shocks is higher compared to the halo being subjected to the right amount of radiative feedback to slow down star formation (K. Inayoshi et al. 2018). If star formation is not halted, these motions could instead affect the nature of the stars that formed. By causing turbulence within the halo, these motions enable a substantial fragmentation of the material that in turn could lead to

less extreme masses of the first stars (T. H. Greif et al. 2011).

The mechanism of baryon streaming motion could suppress star formation in dark halo masses up to $10^8 M_\odot$ which is roughly ten times the minimum cooling mass. Halos like this can then form very massive seed black holes and population III star dominated galaxies of $10^6 M_\odot$ (K. Inayoshi et al. 2018).

2.4 Population III galaxies

The prospect of detecting single population III stars in the near future appears bleak (C. Rydberg et al. 2012), but primordial clusters or galaxies presents an opportunity of detecting the joint light from many such stars. The chronologically first galaxies of the universe does however appear to be those made from enriched material. This is due to the fact that galaxies have a higher probability of forming in highly clustered areas. The issue with these areas is that they quickly get polluted by heavier elements as they also contain rapid star formation, with massive population III stars that complete their evolution and contaminate the pristine material in only a few million years. These galaxies can however provide a suitable LW radiation background to halt stellar evolution in nearby, still pristine halos that eventually form population III galaxies. This chain of events leads to chemically less evolved galaxies being younger than the enriched ones (M. Stiavelli & M. Trenti 2010).

How massive a population III galaxy is has an important impact on its luminosity and hence also on its detectability. The predictions made so far on how massive the halo and star content can be give halos with an upper limit of $10^8 - 10^9 M_\odot$ (E. Visbal et al. 2017, H. Yajima et al. 2016) and with stellar masses of $0.8 \times 10^5 - 2.5 \times 10^6 M_\odot$ (H. Yajima et al. 2016, K. Inayoshi et al. 2018).

2.5 Predicted number densities of Population III galaxies

As there are many uncertainties in modeling the origin of the first stars and galaxies, different approaches to the problem can differ significantly in their results. Based on the two different mechanisms for delayed star formation described above, two different values for the number densities of population III galaxies have been predicted.

2.5.1 M. Stiavelli and M. Trenti 2010

Based on Press-Schechter theory of dark matter halo formation, their subsequential merging and in the presence of a Lyman Werner background, M. Stiavelli and M. Trenti (2010) produced the following number densities for pristine galaxies. They concluded from their simulations that the already enriched galaxies do, as suspected, form at an earlier stage and experiences a peak around redshift fifteen, whereas the galaxies of population III stars have their peak at a lower redshift, $z \approx 11$, at a formation rate of $2 * 10^{-8} n_{galaxies} Mpc^{-3} yr^{-1}$, see figure 1a. Figure 1b shows the raw data used in the calculations, that is pushed towards lower redshifts, but provided by the same authors.

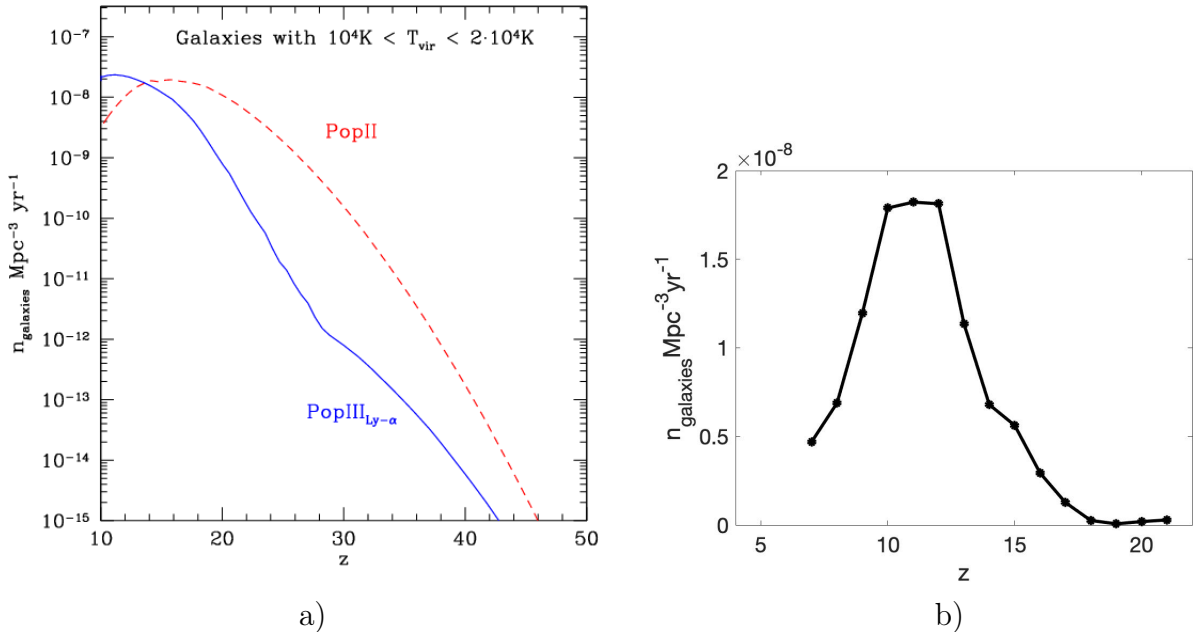


Figure 1: Formation rate of population III and population II galaxies as a function of redshift (M. Stiavelli & M. Trenti 2010)

2.5.2 K. Inayoshi et al 2018

Introducing the above described baryon streaming motions in the simulations for population III galaxies yields a different result compared to that of M. Stiavelli and M. Trenti. These values are given by K. Inayoshi et al (2018). Contrary to the number densities calculated by Stiavelli and Trenti that peaks at $z \approx 11$, these numbers increases or levels out between redshift 10-20, as seen in figure 2. This figure shows number densities of pristine dark matter halos with different viral temperatures. In order

to compare the actual number densities for galaxies the numbers in figure 2 need to be converted to a formation rate. This is obtained by dividing the number densities with the expected lifetime of population III galaxies, which is approximately 10^7 years. This yields formation rates of a maximum of $\approx 3 * 10^{-3} / 10^7 = 3 * 10^{-10} n_{galaxies} Mpc^{-3} yr^{-1}$ which is several order of magnitudes lower than those given in the previous section. Since the results here are given by number densities of massive, pristine dark matter halos it must be transformed to number densities of population III galaxies instead. For this, the prediction that one galaxy per halo will form is used, leaving the numbers unchanged.

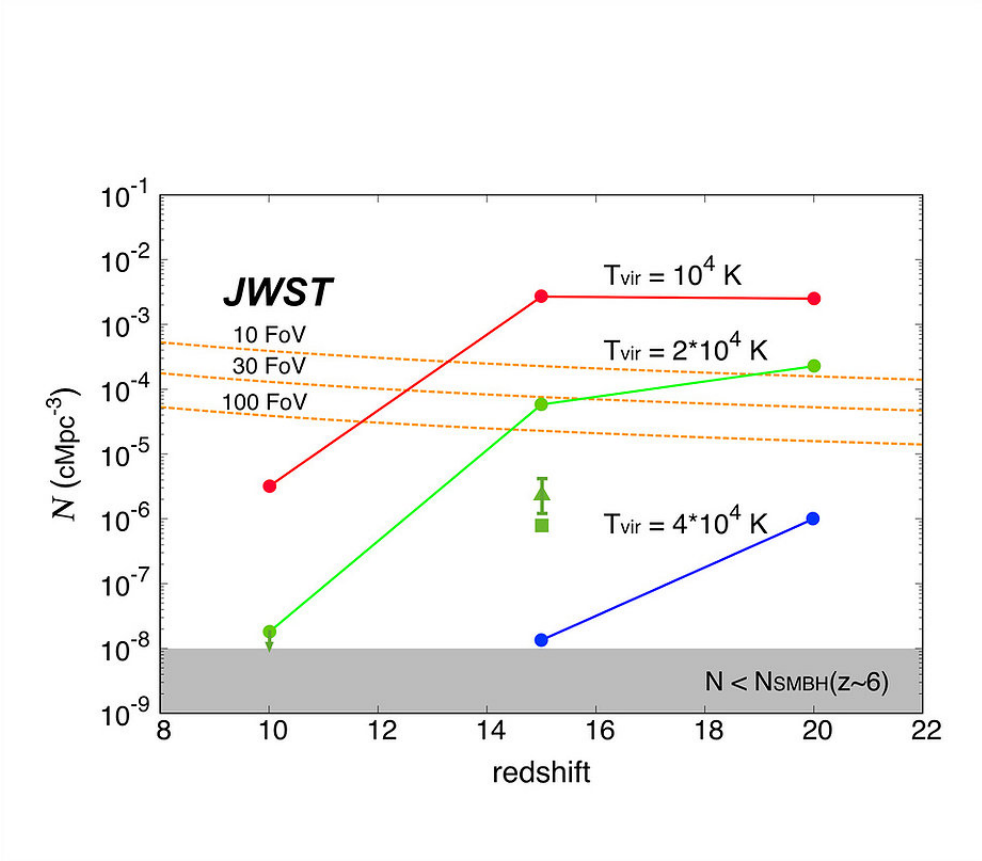


Figure 2: The number densities of massive pristine dark matter halos with different virial temperatures as a function of redshift (K. Inayoshi et al. 2018)

2.6 Characteristics for detection

When searching for population III galaxies it is believed that the emitted light is largely affected by surrounding gas, i.e there is a strong nebular contribution to the spectral

energy distribution. The nebula represents the remains of the material that the stars in the galaxy were made from, so it is unpolluted and also free from metal lines.

Suitable objects need to be identified as population III objects through a couple of predicted qualities. The first major supporting evidence is a spectrum without metal lines, but there are also other radiative characteristics predicted by theory.

2.6.1 Lyman alpha

Population III stars are predicted to be strong emitters of Lyman alpha radiation. These massive stars have higher temperatures which means that electrons have higher velocities and are able to excite hydrogen atoms through collisions, a process that facilitates ionization. This means that the high temperature gives an increase in the overall ionization rate that can be identified through the Lyman alpha radiation released at recombination in the nebula (A. Raiter et al. 2010). However, a significant fraction may be absorbed by the neutral IGM at redshift higher than 6 and reemitted in the form of a very large blob, that may be difficult to detect due to low surface brightness.

2.6.2 He II 1640 Å

The Lyman alpha radiation is in no way unique for stars made from pristine material and can on its own not be used as a confirmation of detection. An additional line to look for is that of He II at 1640 Å. This line originates from the recombination of ionized Helium and was predicted to be strong in pristine stars because of their hard, ionizing spectra producing great amounts of photons above the required energy of 54eV. The situation however seems to be more complicated than this and the luminosity of He II might not be as strong as initially predicted, but it is still one of the best targets for identifying pristine objects (A. Raiter et al. 2010).

The uncertainty that governs the exact behavior of this emission line is due to the various assumptions about the processes that goes into the modeling, such as the shape of the spectra, the hydrogen number densities and the ionization parameter. Exactly how the collisional effects behave with change in metallicity is also a source of uncertainty since it depends on the detailed conditions of the gas. To get more accurate predictions a tailored photoionization model is needed, which is no trivial task to derive (A. Raiter et al. 2010).

3 Gravitational lensing

Light is, just like matter, affected by the force of gravity. This means that as light passes a massive object it gets bent; how much depends on the distance to the massive object also known as a gravitational lens. This phenomenon is described by general relativity where light simply follows what is known as geodesics. These geodesics represent the shortest path for the light to take in a space-time curved by the presence of matter. This means that when lensed light is observed it gives a distorted image of its source: how distorted depends on the geometry of the involved structures.

3.1 Geometry

The basic geometry of a gravitational lens is shown in figure 3, illustrating the connection between the plane of the source, the plane of the lens and finally the observed image plane (P. Schneider 2009).

The equation that describes the deflected angle of light has for deflections around a point mass the following form:

$$\hat{\alpha} = \frac{4GM}{c^2\xi} = \frac{2R_s}{\xi} \quad (8)$$

With G as the gravitational constant, M as the mass of the lens, c is the speed of light and ξ is the impact parameter that simply denotes the distance from the light ray to the lens. Recognizing that the Schwarzschild radius is $\frac{2GM}{c^2}$, the deflection angle can be expressed as a function of the massive object's Schwarzschild radius, R_s , and the impact parameter only (P. Schneider 2009).

For more complicated mass distributions, the vectorial sum from all the different deflections can be used, resulting in the formula:

$$\hat{\alpha} = \sum_i \hat{\alpha}_i = \sum_i \frac{4Gm_i}{c^2} \frac{\bar{\xi} - \bar{\xi}_i}{|\bar{\xi} - \bar{\xi}_i|^2} \quad (9)$$

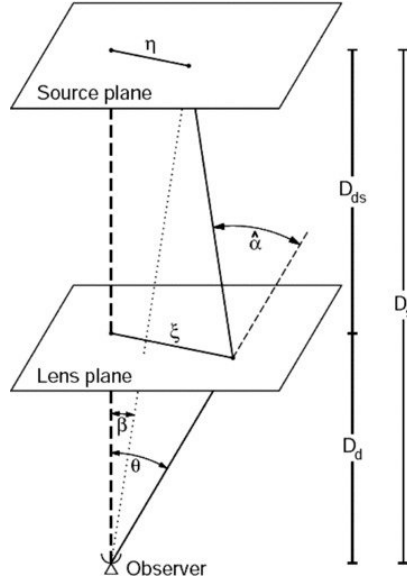


Figure 3: Sketch of a typical gravitational lensing system with the source plane, lens plane and the plane of the observer (Bartelmann & Schneider, 2001).

The deflection angle can then be used to obtain the lens equation that relates the observed position of a source to its true position. The geometry in figure 3 results in an equation for the true position, η , of the source:

$$\bar{\eta} = \frac{D_s}{D_d} \bar{\xi} - D_{ds} \hat{\alpha}(\bar{\xi}) \quad (10)$$

$$\bar{\eta} = D_s \bar{\beta}, \quad \bar{\xi} = D_d \bar{\theta} \quad (11)$$

$$\bar{\beta} = \bar{\theta} - \frac{D_{ds}}{D_s} \hat{\alpha}(D_d \bar{\theta}) \quad (12)$$

Where D is given by the angular diameter distance, since this relates transverse distances with angles. These equations can be manipulated further, exchanging mass for surface mass density that is dimensionless and from this obtain a scaled deflection angle, but the full extent of these equation is beyond the scope of this report.

If equation 11 solves for more than one value of θ , multiple images or even a closed ring, an Einstein ring, of the source can be observed.

3.1.1 Caustic and critical curves

The caustic and critical curves are tools for describing positions on the source and image planes affected by lensing. The caustic curve is defined on the source plane, differing with different redshifts, and representing where the light from the distorted sources originates (K. Kuijken 2003). When the caustic is mapped through the gravitational lens to the image plane it is called the critical curve instead. It is along this curve extended arcs or even full circles of distorted background sources can be observed.

A schematic view of these two curves is given by figure 4a and b. 4a shows five objects in the source plane and their relation to the caustic curves and 4b shows how these curves and the images of the sources are affected by lensing. The inner, diamond shaped curve in 4a transforms to the outer curve in 4b.

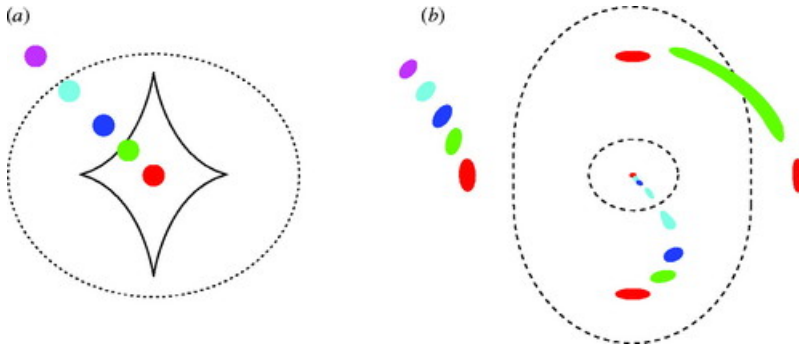


Figure 4: Illustration of critical curves and caustics for an elliptical mass distribution (Narayan & Bartelmann 1999)

3.2 Magnification

Bending light and distorting the image is not the only effect by gravitational lensing, but it also allows for changes in the received flux that can be both magnified or demagnified. This effect is based on the fact that the intrinsic flux from the lensed source is not changed and since gravitational lensing preserves the surface brightness (Tejaswi Venumadhav et al. 2017), it means that as the image gets distorted and changes its shape, the amount of flux that can be observed changes accordingly. This effect can push the receiving flux, that would otherwise not be detectable, above the existing detection limits. In the case of demagnification the opposite happens, but since this is of limited interest for this work the main focus will be on the enhancement of the observed flux.

The problem is that this manipulation of the flux only takes place very near the critical curves of the system. This means that in order for a source to get markedly magnified as it crosses one of these lines it can not be more than a few tens of parsec in size which limits the use of this effects to smaller objects (P. L. Kelly et al. 2018).

4 Next generation telescopes

The light from the first stars of the universe was emitted at very high redshifts which means that the light we observe is strongly shifted towards longer wavelengths. For stars that emit most of their light in the optical to ultra violet part of the spectra it means that the observed light will be found in the infrared region.

Three upcoming telescopes with suitable capabilities in the infrared part of the electromagnetic spectra are the Wide Field InfraRed Survey (WFIRST), the James Webb Space Telescope (JWST) and the Euclid telescope. They will be described briefly in the following sections.

4.1 WFIRST

WFIRST is a project managed by NASA and it is planned to be launched in the mid 2020s. It is meant for research within the areas of dark energy, exoplanets and infrared astrophysics. It consists mainly of two parts; the wide field instrument and the coronagraph instrument. The first of these instrument is the background for the nickname of the telescope being “Hubbles wide-eyed cousin”, since it provides a field of view a hundred times that of the Hubble telescope even though it has the same size. It will collect the light from a billion different galaxies during its lifetime and will be used to construct a microlensing map of the surveyed sky. The coronagraph is meant for more detailed observations with high contrast imaging and detailed spectroscopy, especially of nearby exoplanets. The telescope will operate in the range of 0.48-2.00 μm (R. Goullioud et al. 2014).

4.2 JWST

The James Webb space telescope is a collaboration between NASA, ESA (European Space Agency) and CSA (Canadian Space Agency) and it is meant to be the successor of the Hubble telescope, which it will exceed in both resolution and sensitivity. It will operate in the interval of 0.6-28 μm and will be used for the study of every phase in the evolution of the universe, from the very first light to systems able of hosting possible life-supporting planets.

It contains four instruments; the Near-Infrared Camera (NIRCam), the Near-Infrared Spectrograph (NIRSpec), the Mid-Infrared Instrument (MIRI) and the Fine Guidance Sensor/Near InfraRed Imager and Slitless Spectrograph (FGS/NIRISS) (J.P. Gardner et al. 2006).

	Photometric depth (m_{AB})	Survey Area (deg^2)	Spectroscopic depth ($erg\ s^{-1}cm^{-2}$)
WFIRST	28	20	$4.2 * 10^{-17}$
Euclid	26	40	$3 * 10^{-16}$
JWST	30	0.0810	see table 2

Table 1: Detection limits for the different telescopes

Field of View (FoV)	Time (h)	Survey Area (deg^2)	Spectroscopic depth ($erg\ s^{-1}cm^{-2}$)
1	100	0.0036	$2 * 10^{-19}$
10	10	0.036	$6 * 10^{-19}$
100	1	0.36	$9 * 10^{-18}$

Table 2: JWST spectroscopic detection limits for $z=10$, $R=1000$, G235M grism and a line width of 100 km/s

4.3 Euclid

Euclid is an ESA project meant to provide information about the origin of an accelerating universe. It will gather observations on the morphology, photometry and spectral properties of galaxies in order to obtain a three dimensional map of the matter distribution of the universe. In order to do that it will need both visual and infrared capabilities, with the latter being in the range of 1.0-2.0 μm . The instrument on board will be the Visible imager (VIS) and the Near Infrared Spectrometer and Photometer (NISP) (R.J. Laureijs et al. 2010)

4.4 Detection limits

When observing the first stars and galaxies there are two detection limits of interest. Firstly, in order to detect the object at all, a satisfactory photometric limit is needed. When the object has been detected and selected as a possible candidate for a population III object, a more demanding spectroscopic measurement is required for confirmation of the desired spectral properties.

The different depths of the three telescopes described above are given in Table 1 and 2.

5 Method/Background

The main objective for the calculations done here is to arrive at required number densities and formation rates of population III galaxies for detection. The calculations need to be based on predicted luminosities for population III galaxies; for magnitudes as well as flux from interesting emission lines. These values are provided by the spectral synthesis model Yggdrasil (E. Zackrisson et al. 2011) described below.

Another vital component to the calculations has to do with the behavior of the magnification due to gravitational lensing. Magnification of the received flux will enhance the possibility of detection so the probabilities for different values of magnification is also implemented in the calculations.

5.1 Yggdrasil spectral synthesis model

The model was developed by Zackrisson et al. (2011), using the Schaerer (2002) and Raiter et al. (2010) single stellar populations for population III stars and is designed for modeling the spectral energy distributions of galaxies at high redshifts.

Since the high redshift universe still remains unexplored, the model needs to rely on information provided by a combination of theory and simulations. The individual population III stars in low mass dark halos are most likely undetectable by the currently planned missions and the model is instead concerned with the somewhat later forming population III galaxies, whose integrated signatures stand a better chance of detection.

The model includes nebular emissions and the effect by dust extinction, even if the latter is not included in the calculations performed here. Nebular emission have a big impact on young and star forming galaxies and it increases with decreasing metallicity and is hence of great importance for pristine galaxies. It is predicted that nebular emission dominates the emission for population III galaxies at all redshifts. In order to reduce the contribution by the nebula, a huge fraction of the ionizing radiation produced by the massive primordial stars needs to escape through the surrounding gas and leak out into the intergalactic medium. To break the nebular dominance and bring its influence down to 10% the escape fraction needs to exceed 0.95. For this model the nebula is assumed to be spherical, ionization-bounded and to have a constant hydrogen density.

Another important aspect is the IMF of the pristine stars. The exact form is highly unclear, but as previously mentioned; theory and simulations both point towards these

stars being very massive. This results in a top-heavy IMF, but its peaking mass or slope is still uncertain and determining this is one of the answers that future detections might provide. Previously it was believed that the IMF was indeed very top-heavy and peaked around $100M_{\odot}$ but over time a more nuanced picture has evolved pointing towards a less extreme value. There might also have been two waves of star formation in the pristine universe with the first wave being characterized by very massive stars and the second with stars less extreme. The truth might reside somewhere in between but that remains to be determined. Yggdrasil offers three different IMFs for population III stars:

5.1.1 PopIII.1

This model is based on a Shaerer (2002) Single Stellar Population (SSP) with a power-law IMF ($dN/dM \propto M^{-\alpha}$) of slope $\alpha = 2.35$ in the mass range of $50 - 500M_{\odot}$

5.1.2 PopIII.2

This model differs from that of popIII.1 by in stead using a log-normal IMF with a characteristic mass of $M_c = 10M_{\odot}$. It has a dispersion of $1M_{\odot}$, but the wings of the distribution covers the range of $1 - 500M_{\odot}$.

5.1.3 PopIII Kroupa

This is the same model as the Kroupa IMF used for population I and II stars but with zero metallicity and uses an IMF with a broken power law with $\alpha = 2.3$ above $0.5M_{\odot}$, $\alpha = 1.3$ between $0.08 - 0.5M_{\odot}$ and $\alpha = 0.3$ below $0.08M_{\odot}$. Unlike PopIII.1 and PopIII.2, this is not a top-heavy IMF.

5.1.4 Parameters

Besides the choice of metallicity/IMF, the following parameters also need to be set:

- The cosmology, which is set to $\Omega_M = 0.27$, $\Omega_{\Lambda} = 0.73$ and $H_0 = 0.72 \text{ km s}^{-1} \text{ Mpc}^{-1}$.
- Gas covering factor (f_{cov}) - regulates the relative contribution of the nebula to the total SED of the galaxy. Can be set to 0, 0.5 or 1. This determines the Ly α escape fraction since $f_{cov} + f_{esc} = 1$. Two cases will be investigated here; $f_{gas} = 1$ ($f_{esc} = 0$) and $f_{gas} = 0.5$ ($f_{esc} = 0.5$).

- Star formation history (SFH) - provides the options of instantaneous star burst or constant star formation during 10, 30 or 100 million years. For most calculations a SFH of 10 million years will be used, but a comparison with the case of an instantaneous burst will be performed.
- Photometric system - determines which set of filters used for the output of the results.
- $Ly\alpha$ transmission factor - determines what fraction of $Ly\alpha$ photons that reach the observer by combining the $Ly\alpha$ escape fraction with the absorption fraction of the inter galactic medium. This parameter will not be changed during the calculations performed here, but have a constant value of 0, meaning no transmission of the Ly alpha line due to complete absorption.
- Redshift coverage - the model offers three sets of redshift ranges, either the full range 0-15, or divided into low/high redshifts values. The calculations done here either concerns the whole range or a somewhat shortened range at the low redshift end.

5.2 Magnification data

The magnification data used for the calculations in this report is provided by the work of Zackrisson et al. (2015). Probabilities of magnification were estimated through cosmological simulations, based on the Millenium N-body simulation by Springel et al. (2005), that mapped the matter distribution of the universe up to redshift 10. This matter distribution was then projected onto 52 selected lens planes and from this the lensing properties of random sight-lines could be calculated.

5.2.1 Inter- and extrapolating data

The probability for magnification was given for four different values of magnification; 10, 100, 1000 and 3000 and for redshift up to 10 (see figure 5a). This could be combined with a data set where the probabilities instead were given for a continuous range of magnifications up to 90000 but at a specific redshift of 9 (see figure 5b), to extrapolate the data in order to obtain the probabilities for magnifications between 0 and 5000 for any redshift between 0 and 15. This was done by applying the shape of the

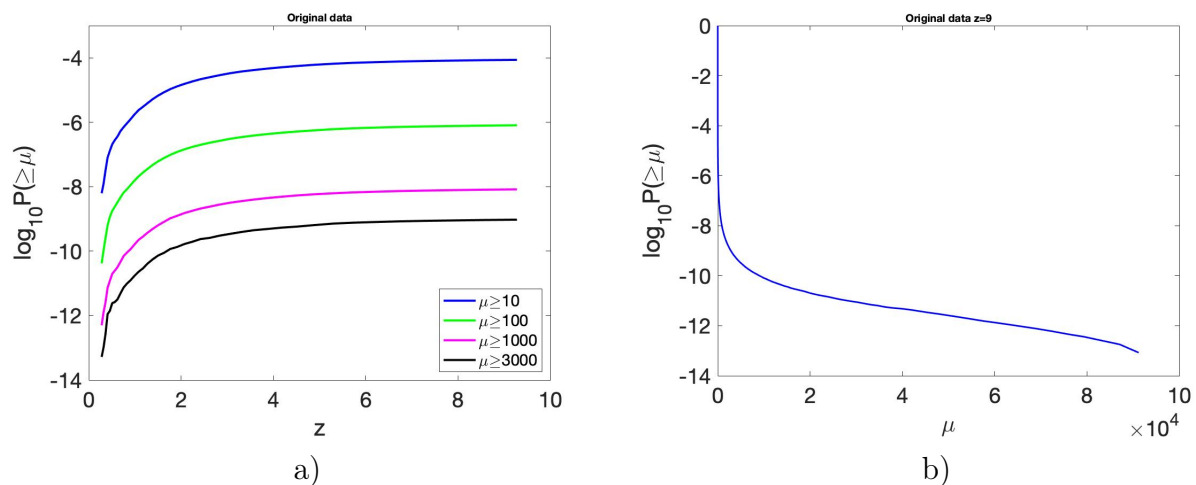


Figure 5: The original magnification data, provided by Zackrisson et al. (2015)

probability-magnitude relation at redshift 9 to the less concentrated data given for only four different magnifications. The relation was assumed to be a power law:

$$P(\geq \mu) \propto \mu^{-2} \quad (13)$$

This relation was applied to the data showed in figure 5a which were fitted to a power law at each redshift. The four resulting formulas, one for each given magnification, were then inter- or extrapolated to a chosen magnitude. This resulted in a function that gave the probability for any magnification at any $z \leq 15$. This function was then tested on the probability data given for a constant redshift of 9 from fig 5b, and the result is illustrated in figure 6.

Figure 7 shows the result from the intra- and extrapolation in comparison with both the data at redshift 9 and the data for the fixed magnification. The four solid lines represents magnifications of 10, 100, 1000 and 3000 as given by the created function and the stars along these lines are the originally provided probabilities for the same magnifications. The dotted lines shows the result for additional magnifications (5, 25, 50, 500 and 2500) and the red crosses are the given probabilities for magnification at redshift 9 to further compare the results. The largest difference between the generated function and the given data is seen at low magnifications. At magnification 10 and 50, the deviation has a maximum at $\approx 15\%$ and for higher magnifications this difference decreases to $\lesssim 5\%$.

The inter- and extrapolating function was used in all following calculations making

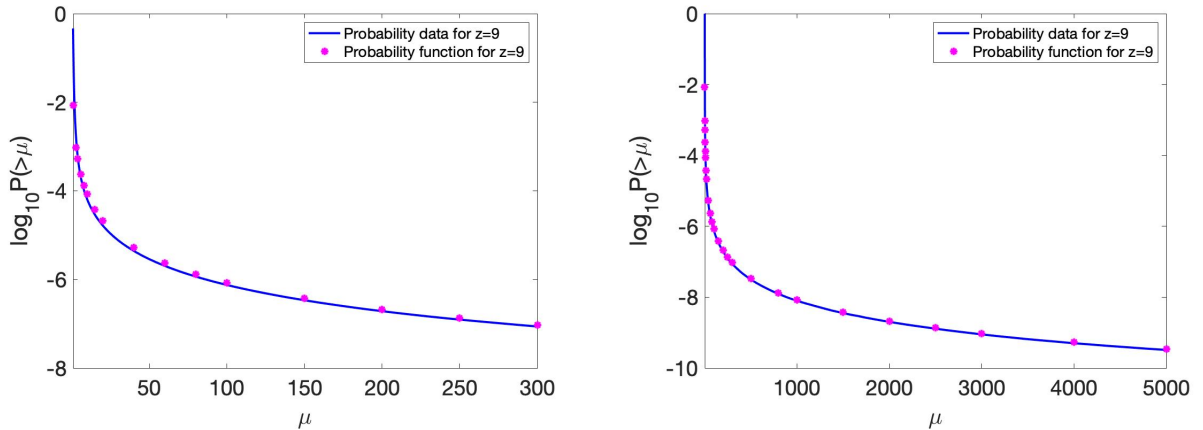


Figure 6: Results from the interpolation of the data at redshift 9 in comparison with the given data.

it possible choose both magnification as well as redshift freely within the outer limits.

5.3 Equivalent width of He II

The flux of He II 1640 is calculated by combining the continuum emission from Yggdrasil at 1640 Å with the equivalent widths predicted by Raiter et al. (2010), see figure 8. Each line represents a different IMF and the values for PopIII.1 (yellow), PopIII.2 (red) and PopIII Kroupa (black) are approximately 90, 40 and 20. To include a margin of error to these values, a factor of three was used giving different equivalent widths of 30, 90 and 270 for PopIII.1, 40/3, 40 and 120 for PopIII.2 and finally 20/3, 20 and 60 for PopIII Kroupa. These equivalent widths are then multiplied with the predicted continuum flux at 1640 Å for the different models in order to obtain the flux of the emission line.

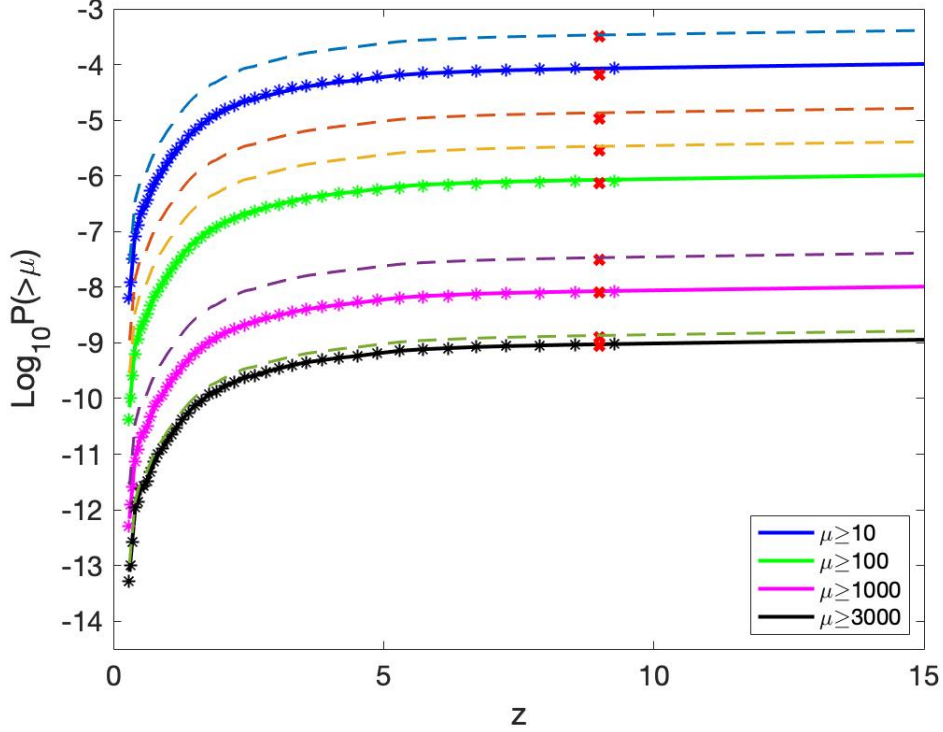


Figure 7: Inter- and extrapolation function of data compared to the given data at all redshifts. The solid lines represent the given data for four different magnifications (10, 100, 1000 and 3000) and the red crosses are the probabilities at $z=9$. The broken lines shows the probabilities given by extra- and interpolation of the power law at the additional magnitudes of 5, 25, 50, 500 and 2500. The largest difference between the generated function and the given data is seen at low magnifications. At magnification 10 and 50, the deviation has a maximum at $\approx 15\%$ and for higher magnifications this difference decreases to $\lesssim 5\%$.

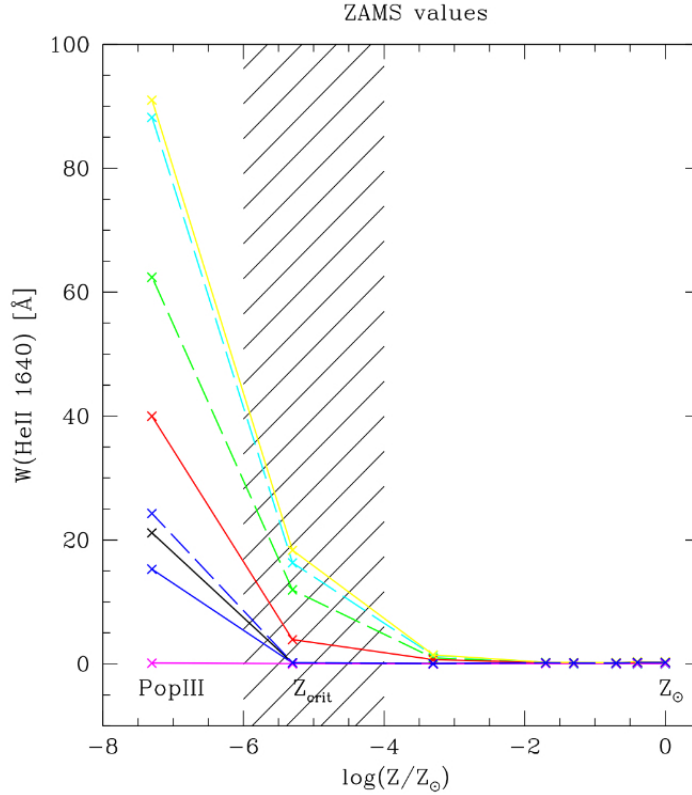


Figure 8: Equivalent widths for very young bursts ($<1\text{-}2\text{Myr}$) given by Raiter et al. 2010. The different models are represented as follows: PopIII.1 (yellow), PopIII.2 (red) and PopIII Kroupa (black).

5.4 Estimating the detectability of Pop III galaxies

The detectability of population III galaxies is given through number densities or formation rates needed to obtain enough magnification by gravitational lensing to reach the limit of the chosen telescope. The result is obtained through a few straightforward steps:

- Inter- and extrapolating probabilities for magnification
- Implementing data from Yggdrasil for chosen models and parameters
- Selecting age of the system
- Scaling for the desired mass
- Comparing to the observational depth of telescopes

- Calculating the required magnifications needed for detection and obtaining the probabilities for those magnifications
- Calculating the number density in order for obtaining at least one object with the right magnification
- Converting to formation rates by implementing the predicted lifetimes of population III galaxies
- Comparing to predicted limits for formation rate and number densities of population III galaxies

6 Results

6.1 Photometry

6.1.1 Formation rate of population III galaxies as a function of source redshift

The first calculation was to determine the formation rates needed for photometric detection by WFIRST in the H158 band ($1.38 - 1.77\mu m$) for different galaxy masses as a function of redshift. Figures 9a-9c shows the results for the three different models containing four different galaxy masses. A star formation history of 10 million years and a covering factor of 1 was used.

The most luminous of the models, PopIII.1, is also the model that requires the lowest formation rate for detection by WFIRST. In all models there is a difference in two orders of magnitude in the formation rate between objects that differ with one order of magnitude in mass. If all other parameters are held constant then luminosity scales linearly with mass, up to masses of $10^9 M_{\odot}$ (E. Zackrisson et al. 2011). So one order of magnitude in mass represents one order of magnitude in luminosity. If the luminosity is to be magnified by a factor 10, the probability of magnification changes with a factor of 10^{-2} (since $P(\geq \mu) \propto \mu^{-2}$), which translates into two orders of magnitude in the change of the formation rate, as seen in figure 9 a-c.

The result is compared to predicted formation rates in figure 9d. The more optimistic case provided by Stiavelli and Trenti (2010) indicates that population III galaxies are detectable up to redshift 12, provided that the stellar mass is $10^6 M_{\odot}$. The formation rates given by Inayoshi et al. (2018) are too low in comparison with what is required for detection by WFIRST.

6.1.2 Covering factor 1 and 0.5

The covering factor was the first parameter to be manipulated. Figure 10 shows the comparison between a covering factor of 1.0 and 0.5. The star formation history is still 10 million years.

A covering factor of 0.5 means that the escape fraction also is 0.5 which means that 50% of the stellar radiation from the galaxy leaks out into the intergalactic medium and does not contribute to the nebular emissions. This leads to a fainter object which should require a higher formation rate in order to reach the detection limit. This is

indeed shown for all models in figure 10, with the strongest effect at lower redshifts.

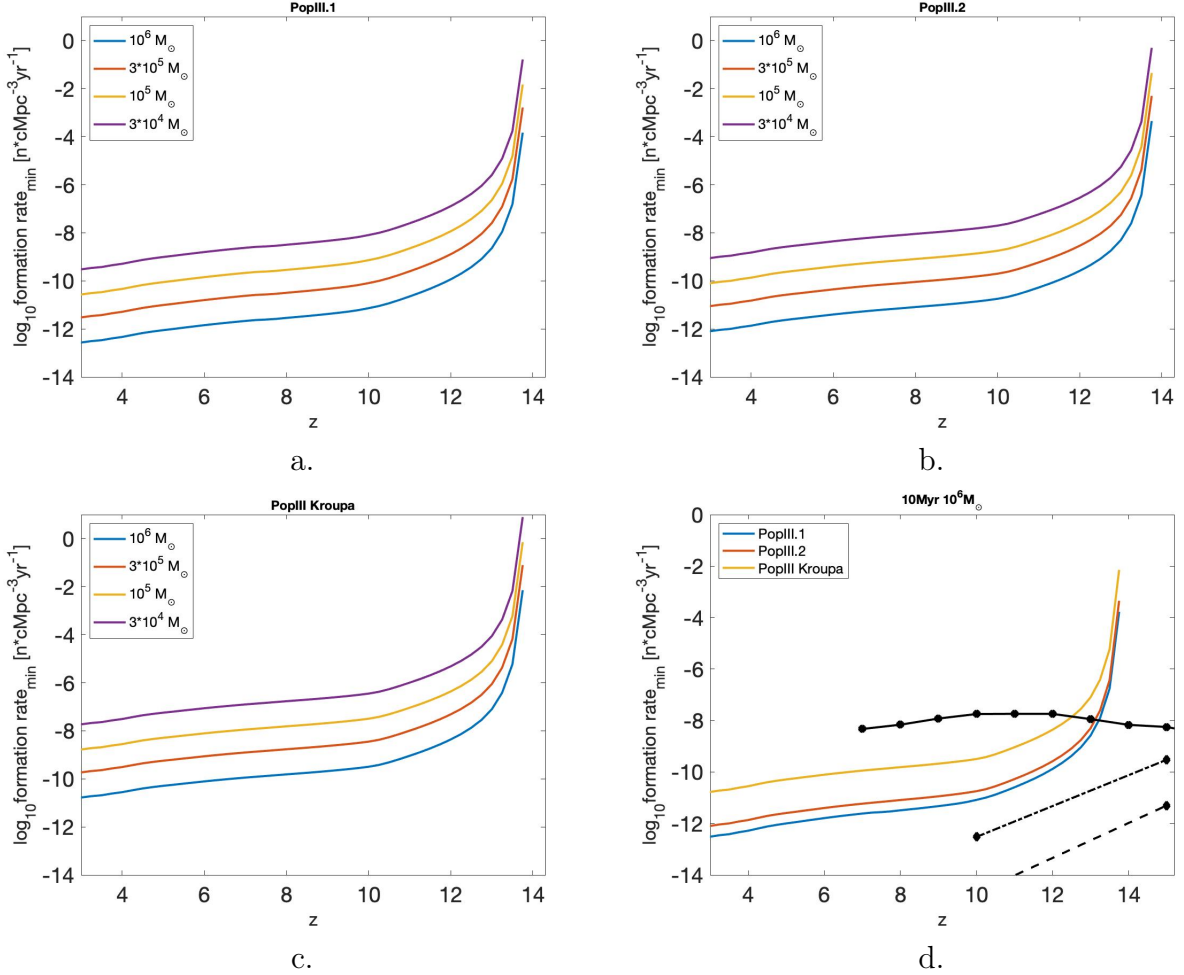


Figure 9: Min formation rate needed for detection by WFIRST (in the H158 band) as a function of source redshift. The top panel and lower left panel (a, b and c) shows the results for the three different IMFs and the lower right (d) shows all models in one figure for $10^6 M_{\odot}$ galaxies in comparison with predicted formation rates by Stiavelli & Trenti (solid black line) and two from Inayoshi (dot-dashed and dashed black line) described in section 2.5.

6.1.3 Star formation history over 10 million years compared to an instantaneous star burst

A constant star formation history was compared to an instantaneous burst for all models at two different ages; 1 and 3 million years (Figure 11) and for PopIII.2 and PopIII Kroupa at two additional ages of 5 and 10 million years (Figure 12). The result is

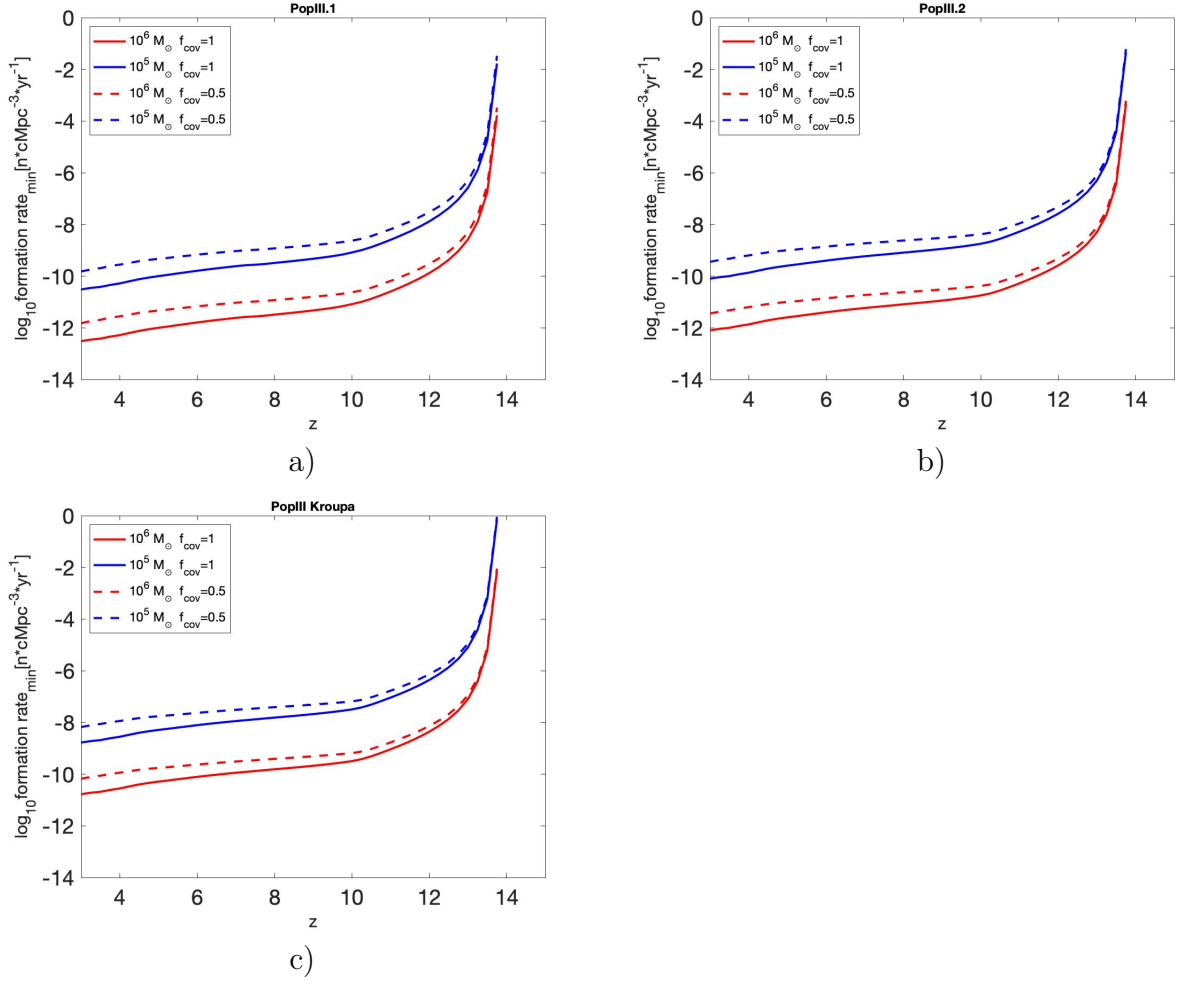


Figure 10: Comparison between covering factor 1 and 0.5 for all three models with masses of $10^5 M_{\odot}$ and $10^6 M_{\odot}$ and star formation over 10 million years. A lower covering factor means that light escapes into the IGM, leaving the galaxies with less luminosity which means that higher formation rates are required for detection.

shown for $10^6 M_\odot$ galaxies. Starting with a very top-heavy IMF as for the PopIII.1 model: when massive stars form instantaneously and evolve rapidly, they live for only a few million years before they have exhausted their fuel. This is reflected in figure 11b that shows a comparison between the two formation rates required at an age of 3 million years. The stars in the instantaneous model has evolved beyond their most luminous state and are either in the giant phase or have already turned supernova or directly collapsed into black holes. Since they are less luminous, a greater star formation rate is needed for detection by WFIRST. At $z = 10$ the formation rate needs to be $\approx 5.6 \times 10^{-12} / 7.1 \times 10^{-13} \approx 8$ times larger in order to enable detection by WFIRST.

For the two other models the difference at 3 million years is not as prominent, due to the lower stellar masses in these models. These stars live longer and it thus takes longer before the difference between an instantaneous burst and 10 million year of constant star formation is visible. In the more top-heavy of the models, PopIII.2, there is a slight shift of the instantaneous case towards higher formation rates, but to see a larger difference ages of 5 respectively 10 million years are considered in figure 12. Now the less massive stars present in these models have had enough time to evolve and the difference between the two different star formation histories becomes clear. After 10 million years the required formation rates are $2.4 \times 10^{-9} / 3.2 \times 10^{-10} \approx 7.5$ (PopIII Kroupa) and $5.2 \times 10^{-10} / 1.8 \times 10^{-11} \approx 29$ (PopIII.2) times higher for the instantaneous model at $z=10$.

6.2 Spectroscopy

After an object is discovered with photometry, spectroscopy is needed to investigate the nature of the object and get details on its spectra that can reveal if it truly is a pristine galaxy. The focus lies on the HeII emission line, predicted to be strong for sources with a hard ionizing spectra. The first step is to obtain the flux of the He II emission line.

6.2.1 HeII 1640 Å flux

Figure 13 and 14 shows the He II fluxes for the three models for three different equivalent widths. These fluxes are calculated without the aid from magnification by gravitational lensing and compared to the spectroscopic detection limit of WFIRST. For the top-heavy models, the flux can be detected for all equivalent widths at low redshifts; $z < 1$. In the most optimistic case with a PopIII.1 model and an equivalent width of 270 (figure 13e), the unlensed flux could be detected up to a redshift of 2 before magnification needs

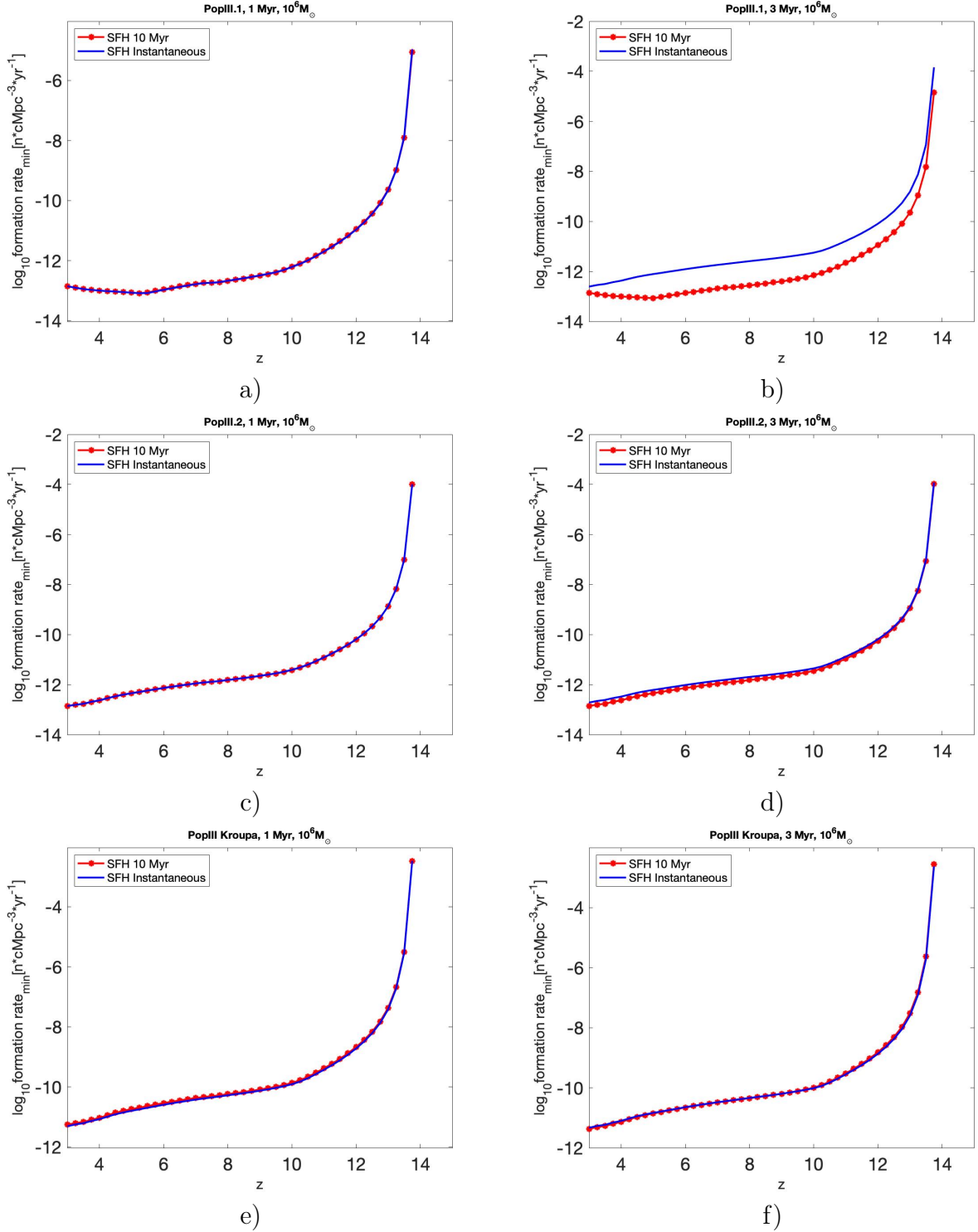


Figure 11: Instantaneous star formation compared to a star formation history of 10 million years for the three different models at ages 1 and 3 million years. The comparison is done for a $10^6 M_{\odot}$ galaxy. At this relatively low age, it is only the most top-heavy of the models that displays a clear difference between the two cases, as seen in b, where a formation rate 8 times as large is needed for detection at $z=10$.

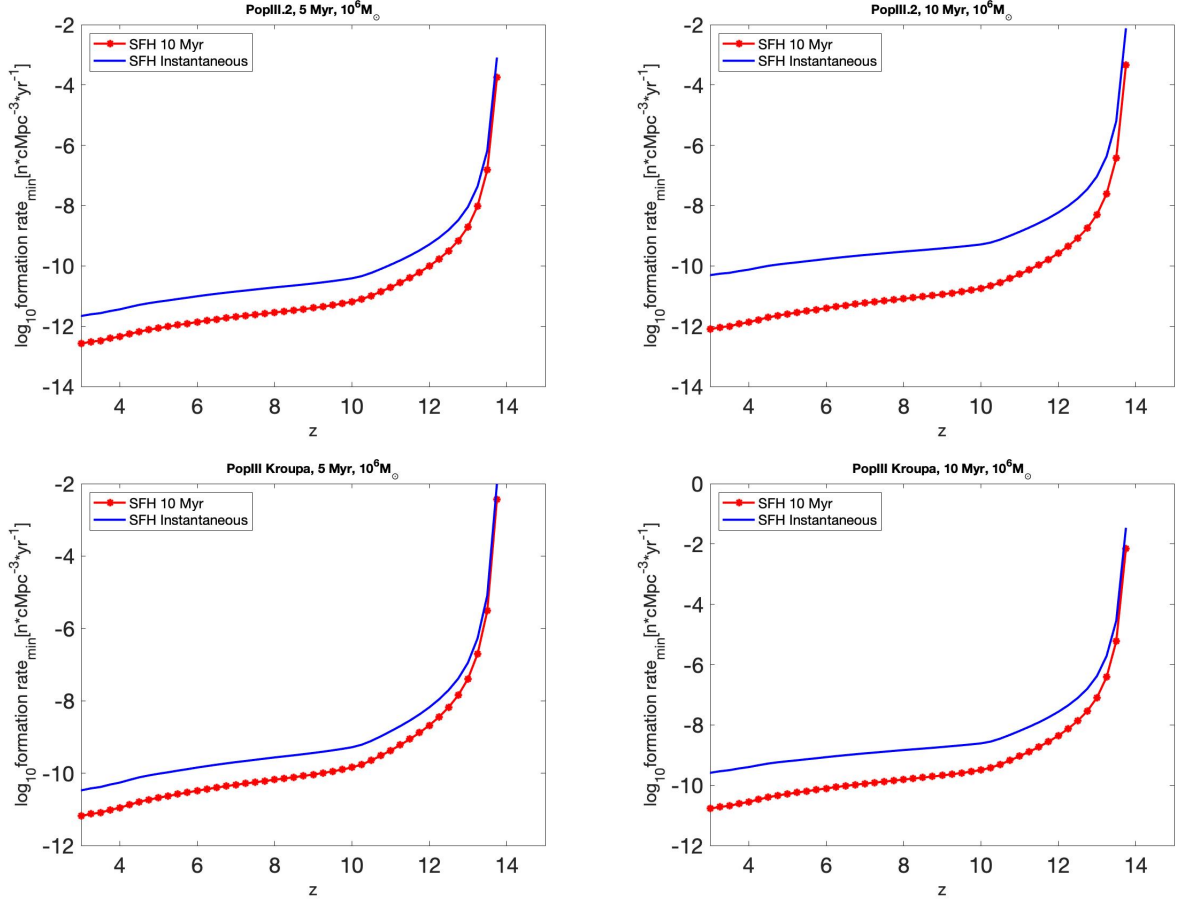


Figure 12: Instantaneous star formation compared to a star formation history of 30 million years for the two model with lower mass stars. The comparison is done for a $10^6 M_{\odot}$ galaxy at ages of 5 and 10 million years. The not so massive stars present in these models have had time enough to evolve leading to a fainter object that requires higher formation rates for detection by WFIRST. At $z=10$ and an age of 10 Myr the required formation rates differ with a factor of 7.5 (PopIII Kroupa) and 29 (PopIII.2) between a constant star formation rate and an instantaneous burst.

to be introduced in order to reach deeper. For the least luminous model, PopIII Kroupa, magnification is important for all redshifts.

6.2.2 Number densities required for detection of He II emission line

The next step is to include magnification by lensing and transform the flux of HeII into number densities required for detection by WFIRST. The result from these calculations is shown in figure 15 and 16. Figures 15a to 15c show the number densities for PopIII.1 models with three different equivalent widths and galaxy masses of $10^5 M_\odot$, $10^6 M_\odot$, and $10^7 M_\odot$. 15c shows a clarification of the predicted number densities that are included in the figures. Looking at the most optimistic case with a PopIII.1 model and an equivalent width of 270, even a $10^5 M_\odot$ galaxy could be detected at redshift 7 and a $10^6 M_\odot$ galaxy could even be detected up to a redshift of 16 when compared to the number densities predicted by Stiavelli and Trenti. For the Inayoshi number densities, $10^7 M_\odot$ galaxies are needed to enable detection. In comparison with the photometric results obtained in section 6.1.1, that points towards galaxies with mass $10^6 M_\odot$ being detectable to $z \lesssim 12$, the case with an EW=270 that results in the same galaxies ($10^6 M_\odot$) being spectroscopically detectable to $z \lesssim 16$ appears too optimistic.

For the two models with IMFs with lower stellar masses (PopIII.2 and PopIII Kroupa), the number densities required for detection increases, but they are still in the range of the predicted values of Stiavelli and Trenti, provided that the galaxy masses and the equivalent widths are large. The less optimistic number densities predicted by Inayoshi et al. is however below the limits of detection even for the most massive galaxies.

6.3 Comparing detectability

Different galaxy masses give different luminosities and hence require different amounts of magnification to reach detectability. These magnifications result in specific number densities in order to have at least one detectable object at the different luminosities (masses). For luminosities below the detection limits of the telescope, a certain magnification is as well needed to enable detection, which also translates into required number densities. A combination of these two is shown for both photometry and spectroscopy in figure 17-23 at specific redshifts of 5, 10 and 13 and for a set of masses ($3 * 10^4 M_\odot$, $10^5 M_\odot$, $3 * 10^5 M_\odot$, $10^6 M_\odot$). The required number densities are constant until the

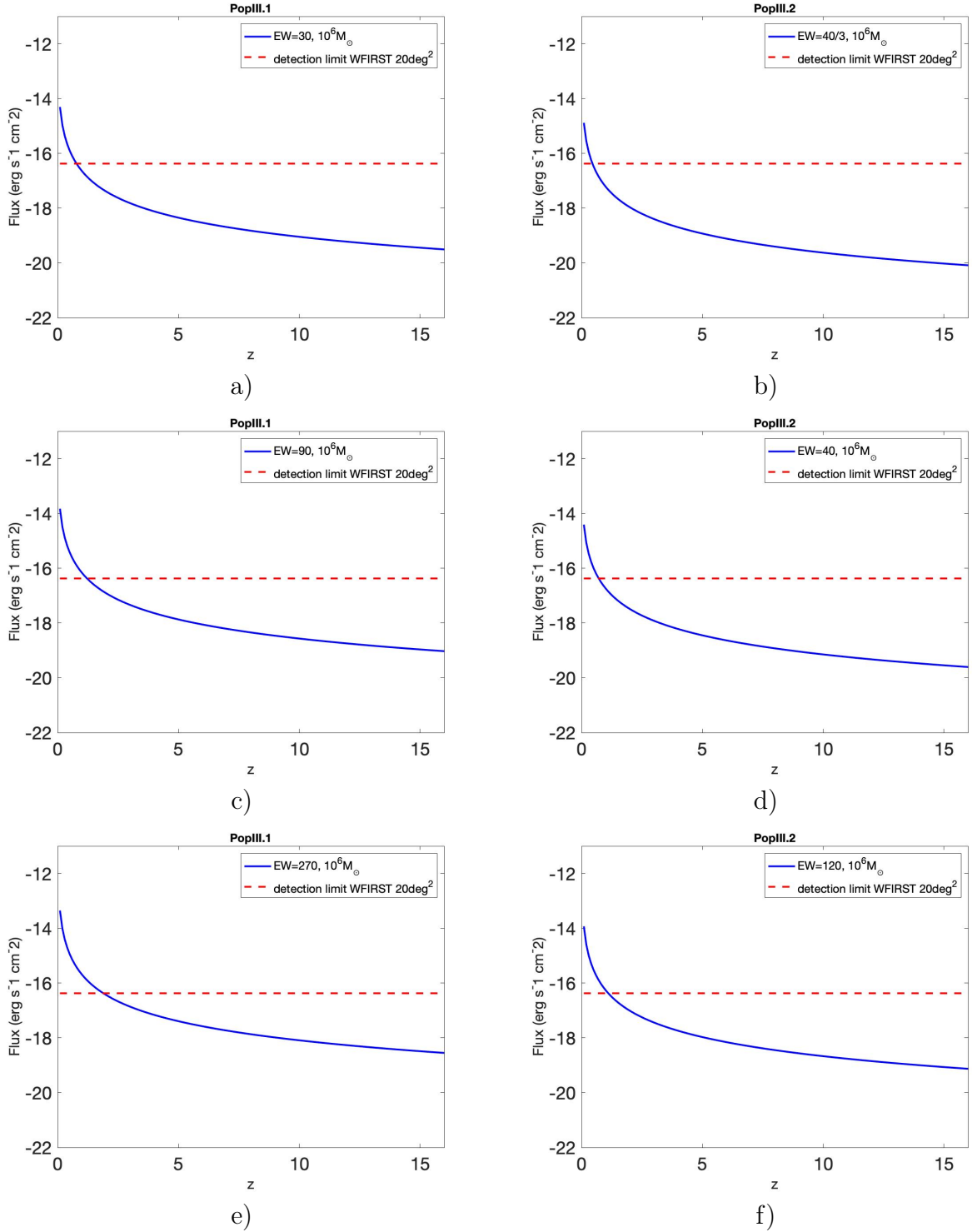
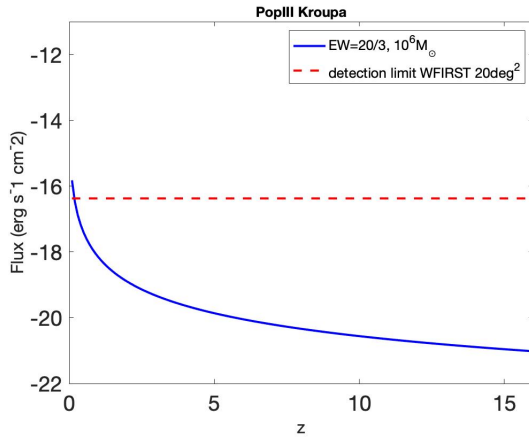
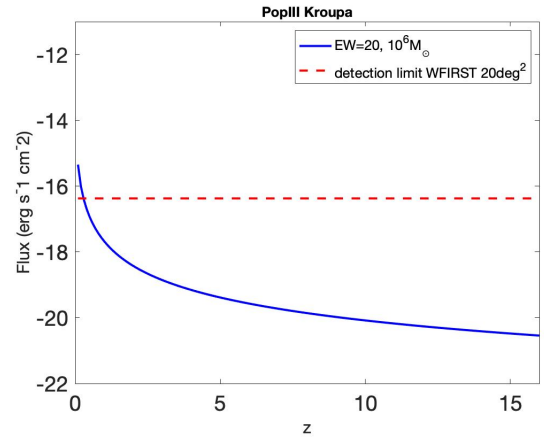


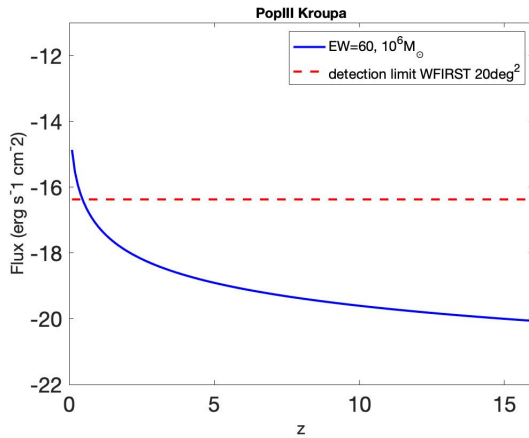
Figure 13: Calculated flux of HeII emission line for PopIII.1 and PopIII.2 models for different equivalent widths as a function of redshift (blue lines). The spectroscopic detection limit of WFIRST is included as the red, dashed line. For low z , unlensed flux appears to be detectable by WFIRST, but in order to reach deeper than $z \gtrsim 1$ magnification is needed.



a)



b)



c)

Figure 14: HeII fluxes for the PopIII Kroupa model (blue lines). The fluxes in this model do not reach the spectroscopic detection limit of WFIRST (red, dashed line)

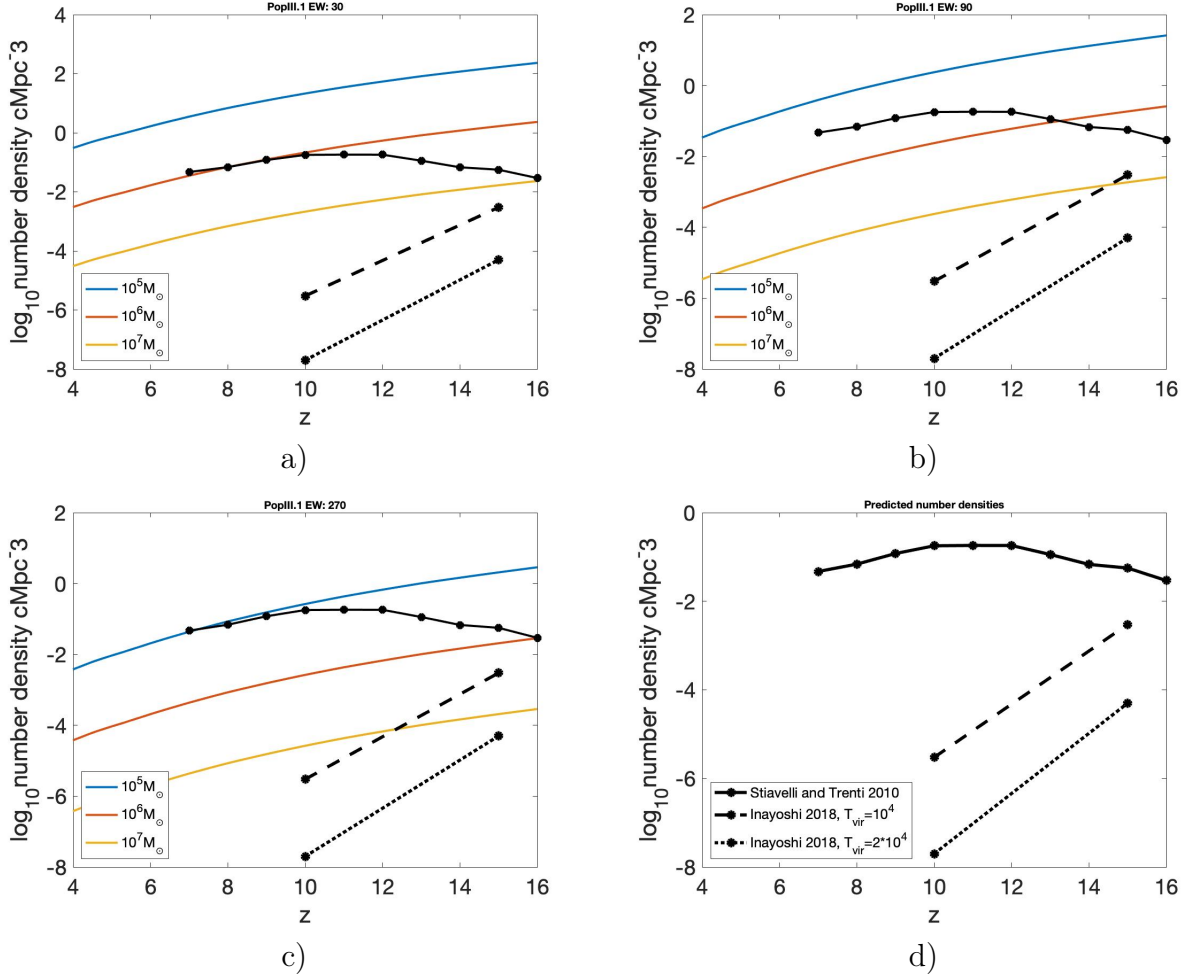
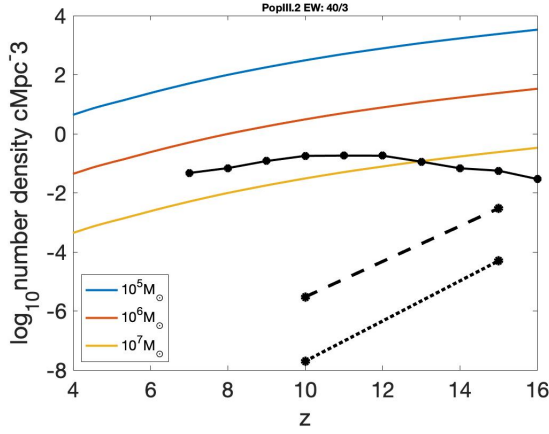
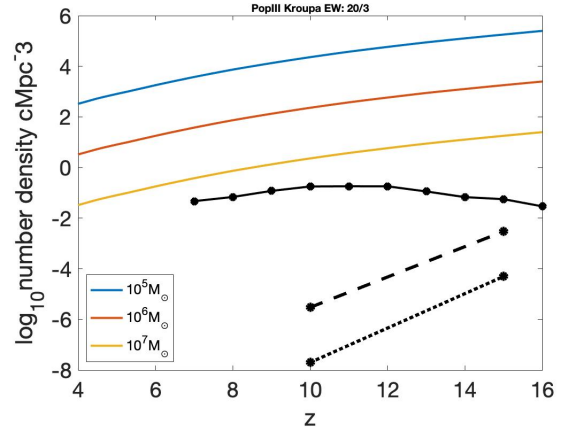


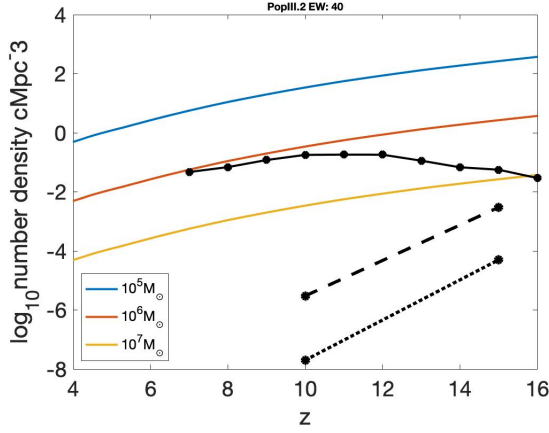
Figure 15: Minimum number densities required for detection by WFIRST for PopIII.1 model with different values of EW in comparison with predicted number densities. In the most optimistic case shown in c), with an EW of 270, the predicted number densities (black lines) exceeds the ones required for detection for the larger masses.



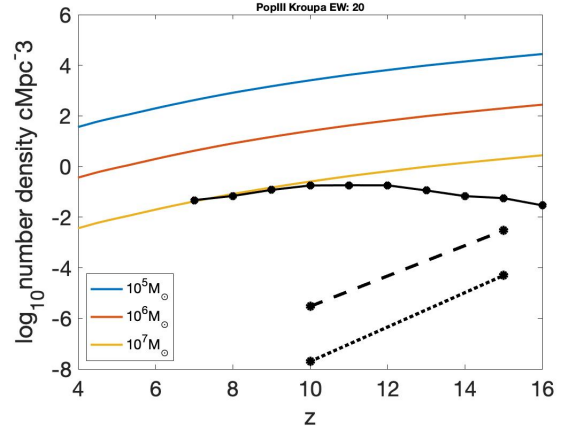
a)



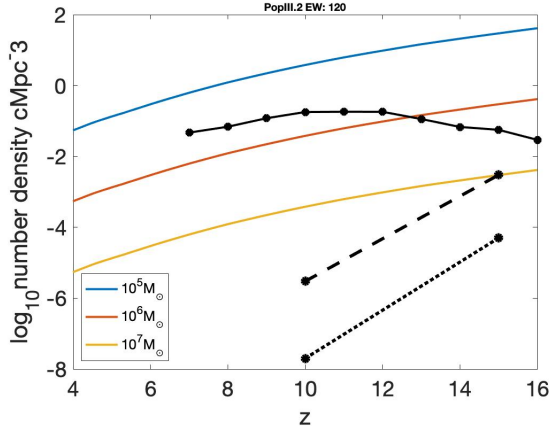
b)



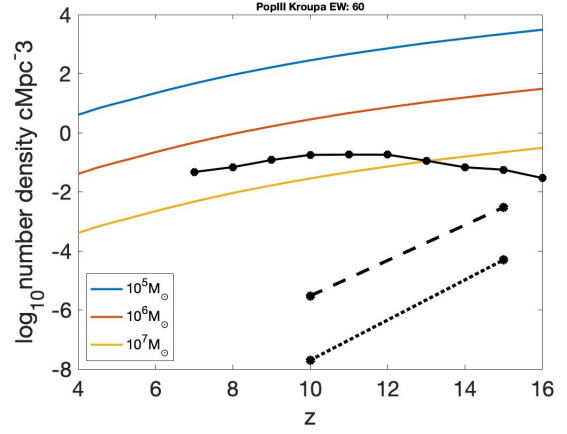
c)



d)



e)



f)

Figure 16: Min number densities required for detection of He II emission line by WFIRST for PopIII.2 and PopIII Kroupa models, with different values for the equivalent width, in comparison with predicted number densities. For these models, the chances of detection requires galaxies of very large masses in combination with large EW for the emission line.

depth of each telescope is reached and after that magnification is needed to enable detection, requiring higher number densities.

6.3.1 Photometry

Figure 17 shows the difference between the PopIII.1 and PopIII.2 models in the photometric case. At the lowest redshift of 5 (fig 17 a and b), JWST is predicted to be the most advantageous telescope for detecting galaxies with masses of $10^6 M_{\odot}$. For the most luminous case of a PopIII.1 model and a redshift of 5, a $10^6 M_{\odot}$ galaxy could presumably be detected without the aid by gravitational lensing.

For lower masses and higher redshifts, JWST is surpassed by WFIRST, which in comparison requires the lowest number densities for detection. Euclid is, with its relative shallow depth of $26 m_{AB}$, in spite of its large survey area, the telescope that would require the highest number densities for detection in all cases considered. For the PopIII Kroupa model, as illustrated in figure 18, WFIRST is preferred in all cases and for all masses.

6.3.2 Spectroscopy

Performing the same comparison between the telescopes for the spectroscopic detection of the He II emission line yields the results presented in figures 19-23. Here, all three different spectroscopic limits of JWST presented above in table 2 are incorporated, with the solid line representing the lowest detection limit. In all cases considered here, the JWST is the most advantageous one for both of its lower limits. The use of the highest detection limit for JWST results in WFIRST being the preferred telescope for detection.

In figures 19 and 20, the middle values for the equivalent widths have been used whereas in figures 21-23 the cases of the lowest and highest equivalent widths are shown for each model. The same redshifts as for the photometric comparison ($z=5, 10$ and 13) has been used. Figure 19 compares PopIII.1 and PopIII.2 models at equivalent widths of 90 (PopIII.1) and 40 (PopIII.2). At the lowest redshift of 5, both models enable detection of a $10^6 M_{\odot}$ galaxy without requiring magnification. For the PopIII.1 model this also includes $3 * 10^5 M_{\odot}$ galaxies. The number densities given before magnification are in the range of the less optimistic values of $\approx 10^{-8} - 10^{-4} cMpc^{-3}$ predicted by Inayoshi et al. (2018). For higher redshifts, magnification is needed and with that the number densities required increases, but for PopIII.1 these number densities are, for

the high mass galaxies, still within the reach of the more optimistic predictions done by Stiavelli and Trenti (2010) of roughly $10^{-2} - 10^{-1} cMpc^{-3}$.

For the PopIII Kroupa model in figure 20, the required number densities increase fast with redshift and galaxies would need to be very massive for the number densities to be able to compare to even the most optimistic predicted values.

For the low and high end values for the equivalent widths, shown in figures 21-23, the result change as one might expect with the broader equivalent widths generating lower number densities and vice versa for the more narrow widths. In the case of a PopIII.1 model (fig 21) and an equivalent width of 270, as shown in figure 21b, galaxies with masses as low as $10^5 M_{\odot}$ at $z=5$ could theoretically be detected by JWST without involving magnification. Figure 22 shows the results for the lowest and highest value of the equivalent width for PopIII.2, a result that resembles that of PopIII.1, but with the required number densities being higher, since the model is fainter. For PopIII Kroupa in figure 23, the smallest equivalent width requires very high number densities to be able to detect even the most massive galaxies. For the larger equivalent width, the outcome is more promising, but the resulting number densities are still high compared to the other two, brighter models.

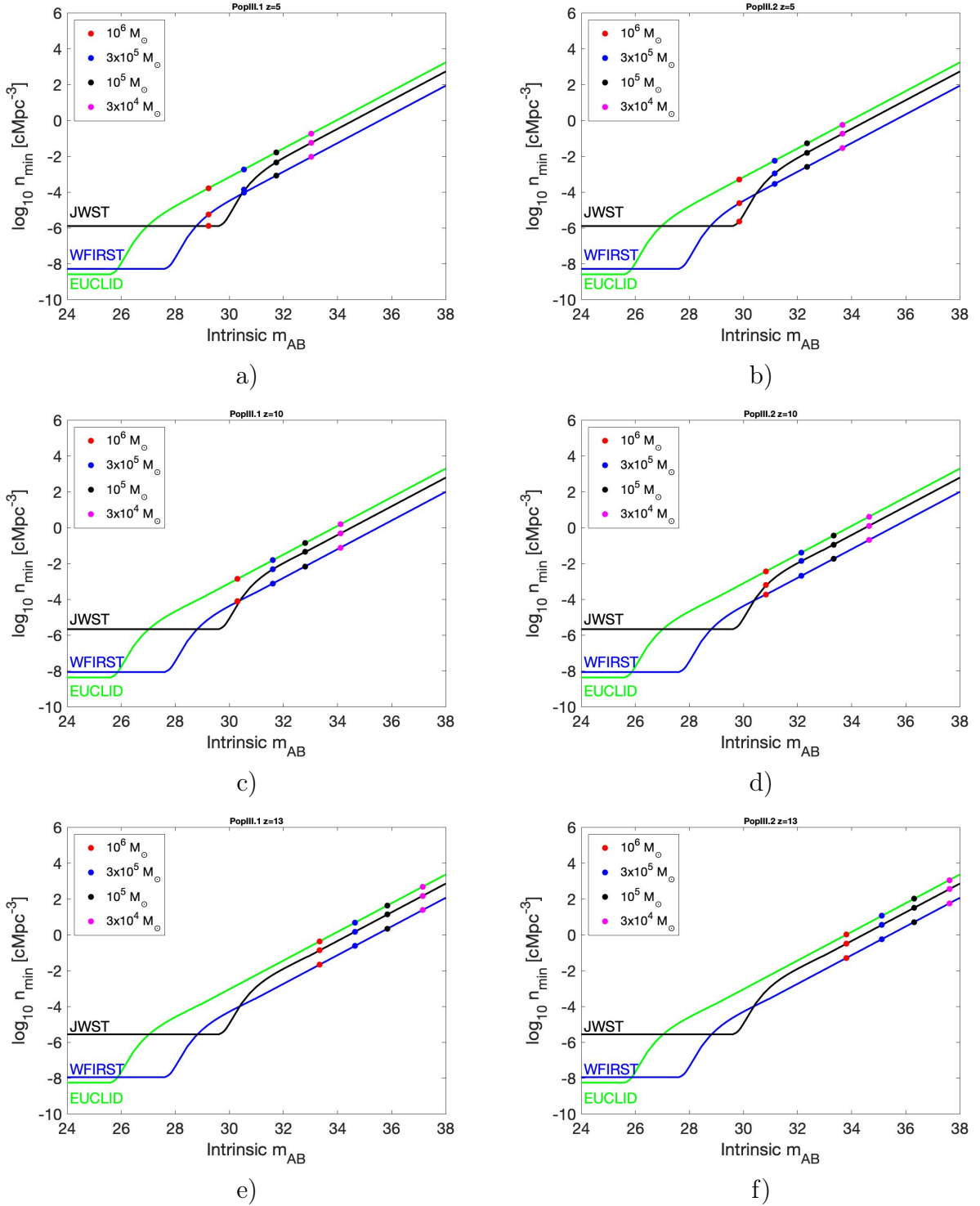


Figure 17: Comparing the photometric detectability of JWST, WFIRST and Euclid for PopIII.1 and PopIII.2 models at redshifts of 5, 10 and 13. When the respective depth of each telescope is reached, magnification by lensing needs to be implemented, this generates larger number densities in order to meet the probabilities for detection. Population III galaxies of different masses, i.e. different luminosities, are illustrated as colored circles. For most redshifts, WFIRST is the instrument that requires the lowest number densities for detection.

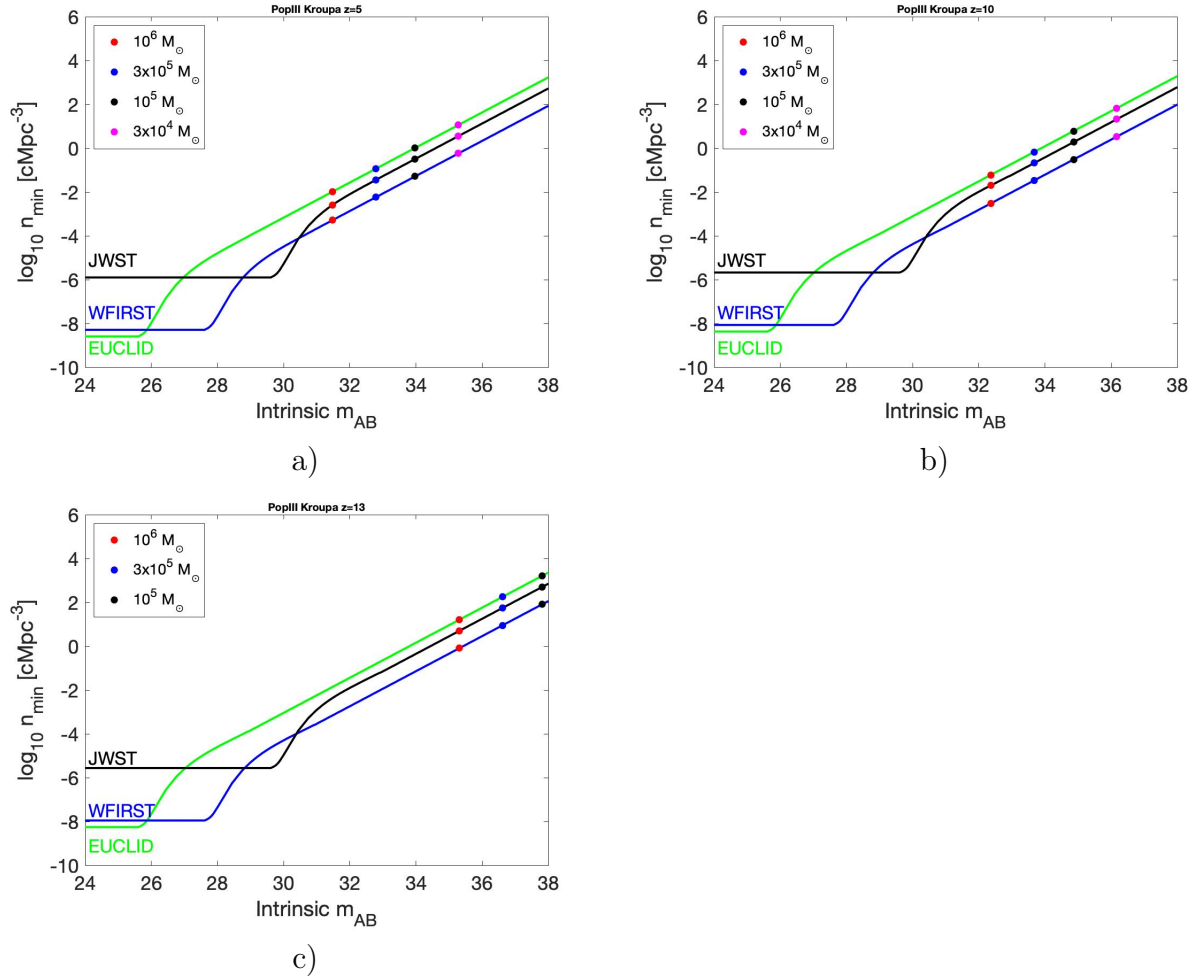


Figure 18: Comparing the photometric detectability of JWST, WFIRST and Euclid for PopIII Kroupa model at redshifts of 5, 10 and 13. For all three cases, WFIRST is the preferred instrument as it requires the lowest formation rates in order to enable detection.

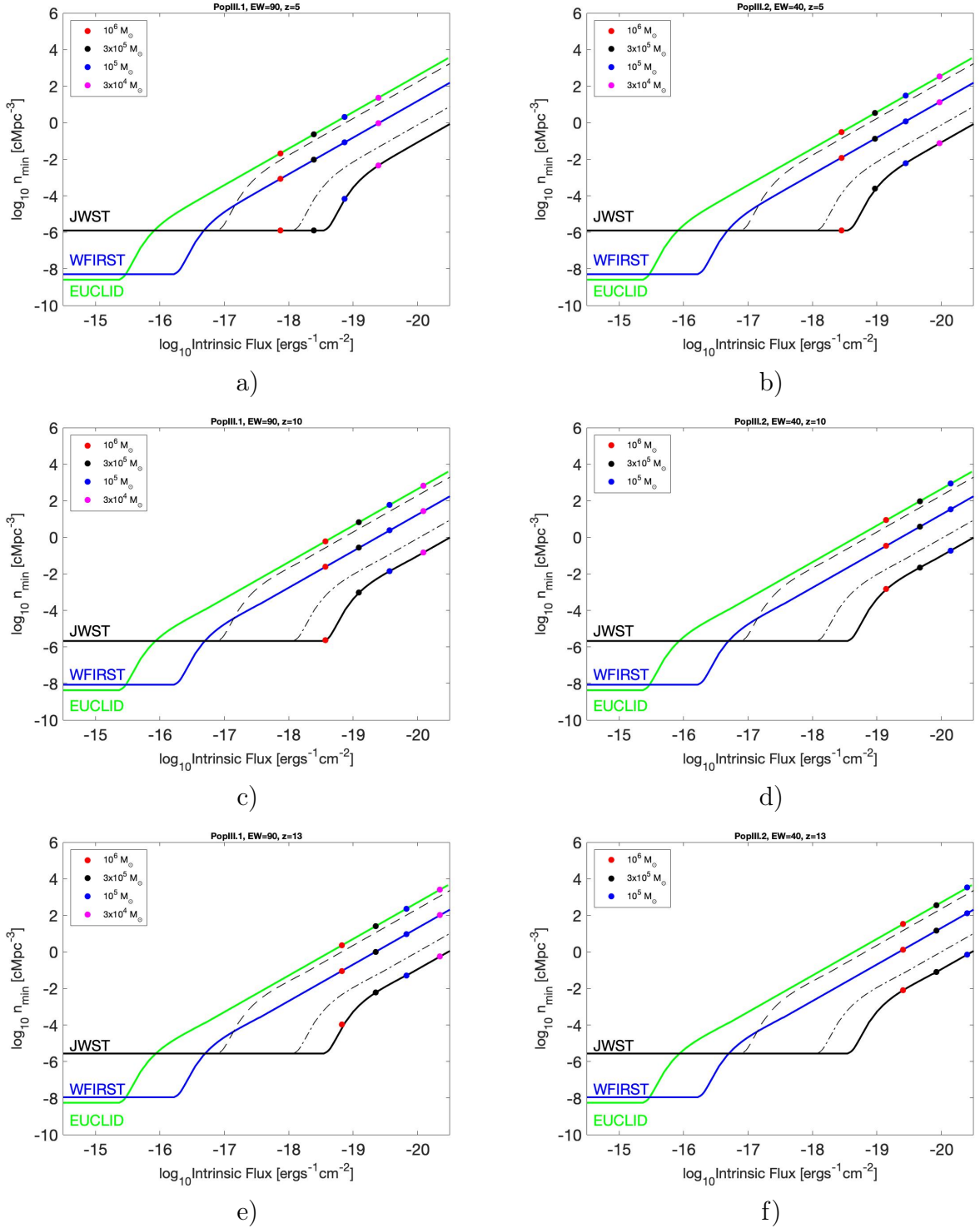


Figure 19: Comparing the spectroscopic detectability of JWST, WFIRST and Euclid for PopIII.1 (EW 90) and PopIII.2 (EW 40) models at redshifts of 5, 10 and 13. The dashed and dot-dashed black lines corresponds to the lower detection limits of JWST from table 2. For all redshifts, JWST is the preferred instrument at the medium equivalent widths used in this figure.

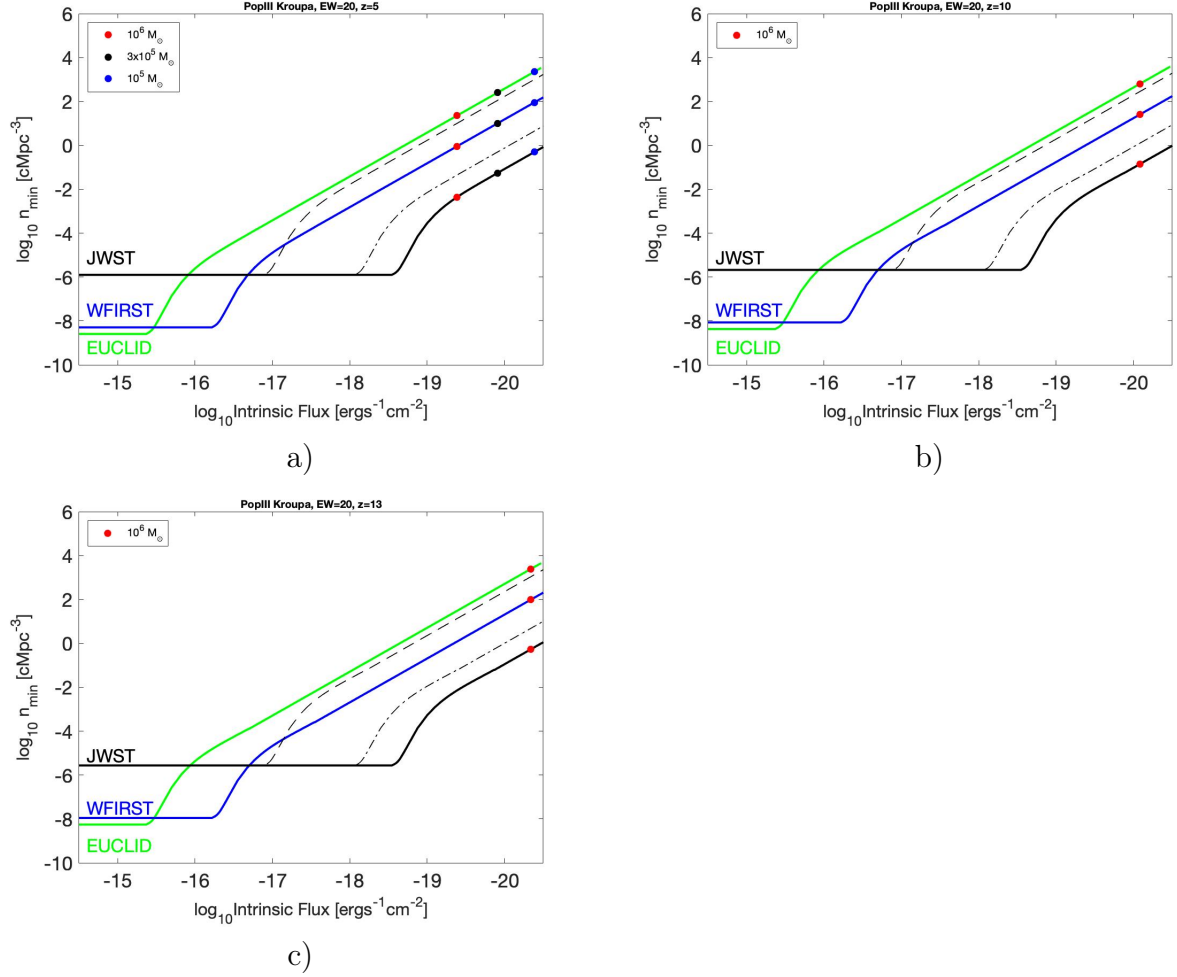


Figure 20: Comparing the spectroscopic detectability of JWST, WFIRST and Euclid for PopIII Kroupa (EW 20) model at redshifts of 5, 10 and 13. The dashed and dot-dashed black lines corresponds to the lower detection limits of JWST from table 2. For all redshifts, JWST is the preferred instrument at the medium equivalent width used in this figure.

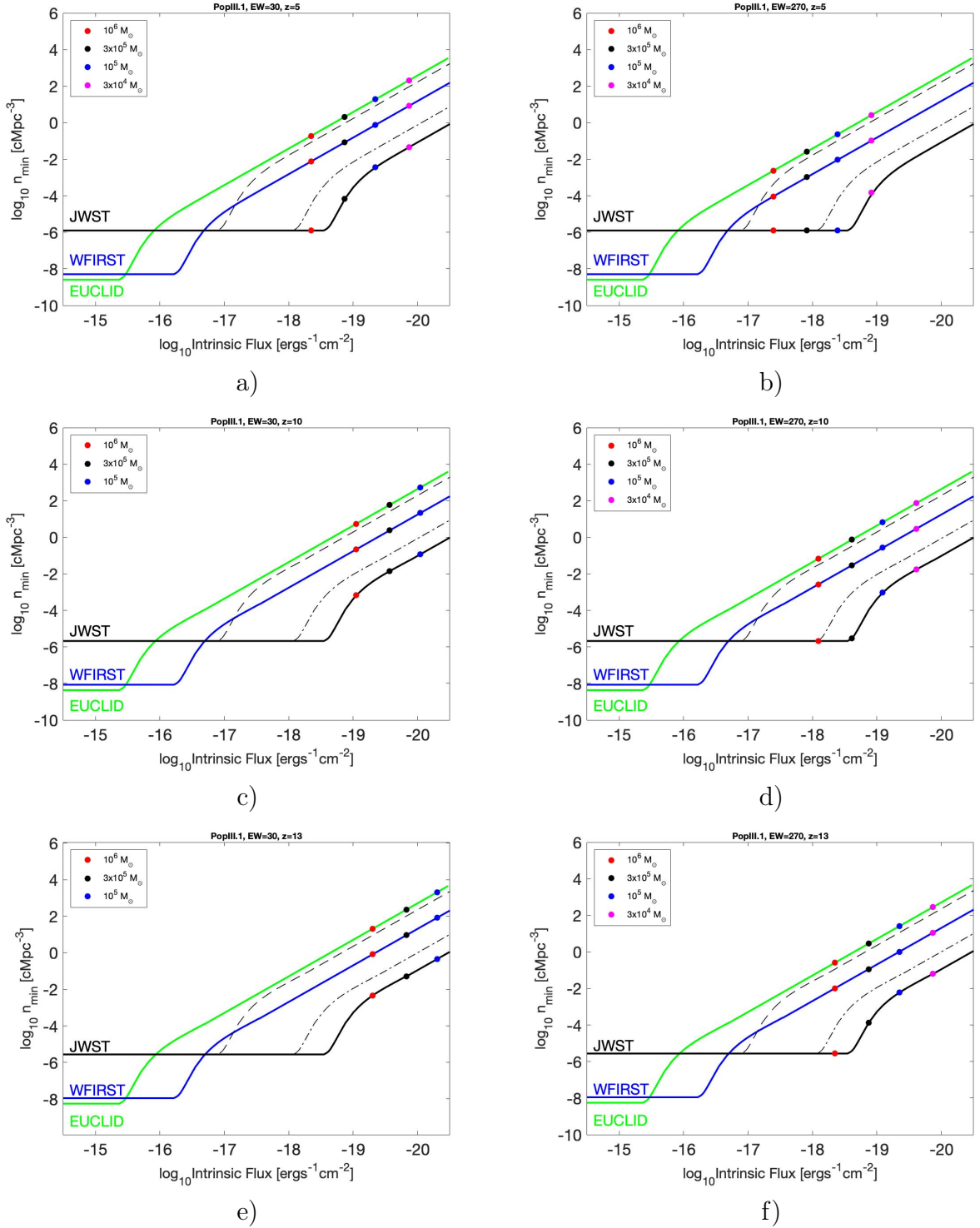


Figure 21: Comparing the spectroscopic detectability of JWST, WFIRST and Euclid for PopIII.1 model with an EW of 30 and 270 at redshifts of 5, 10 and 13. The dashed and dot-dashed black lines corresponds to the lower detection limits of JWST from table 2. For all redshifts, JWST is the preferred instrument for both the lower (30) and higher (270) limit for the equivalent width.

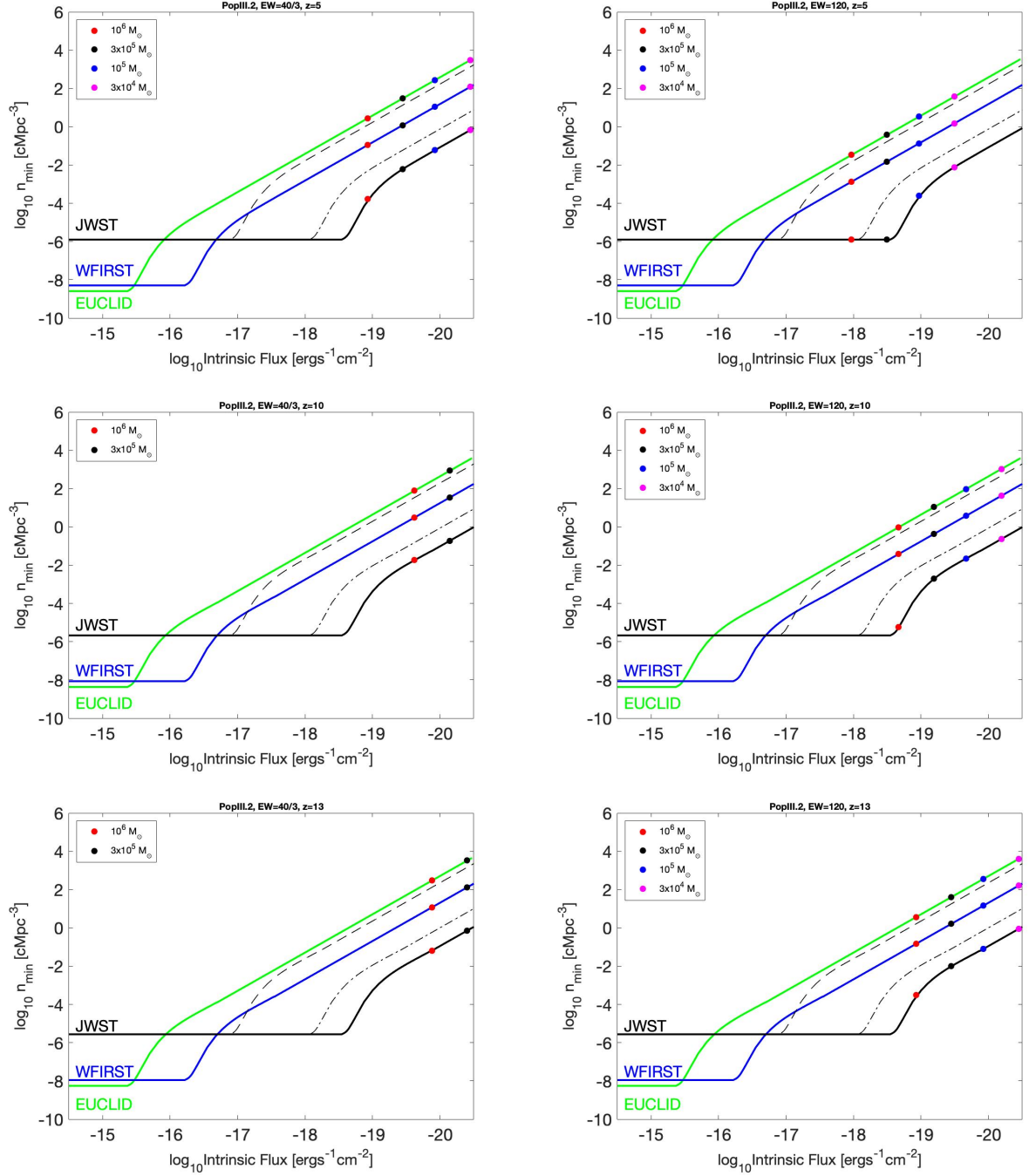


Figure 22: Comparing the spectroscopic detectability of JWST, WFIRST and Euclid for PopIII.2 model with an EW of 40/3 and 120 at redshifts of 5, 10 and 13. The dashed and dot-dashed black lines corresponds to the lower detection limits of JWST from table 2. For all redshifts, JWST is the preferred instrument for both the lower (40/3) and higher (120) limit for the equivalent width.

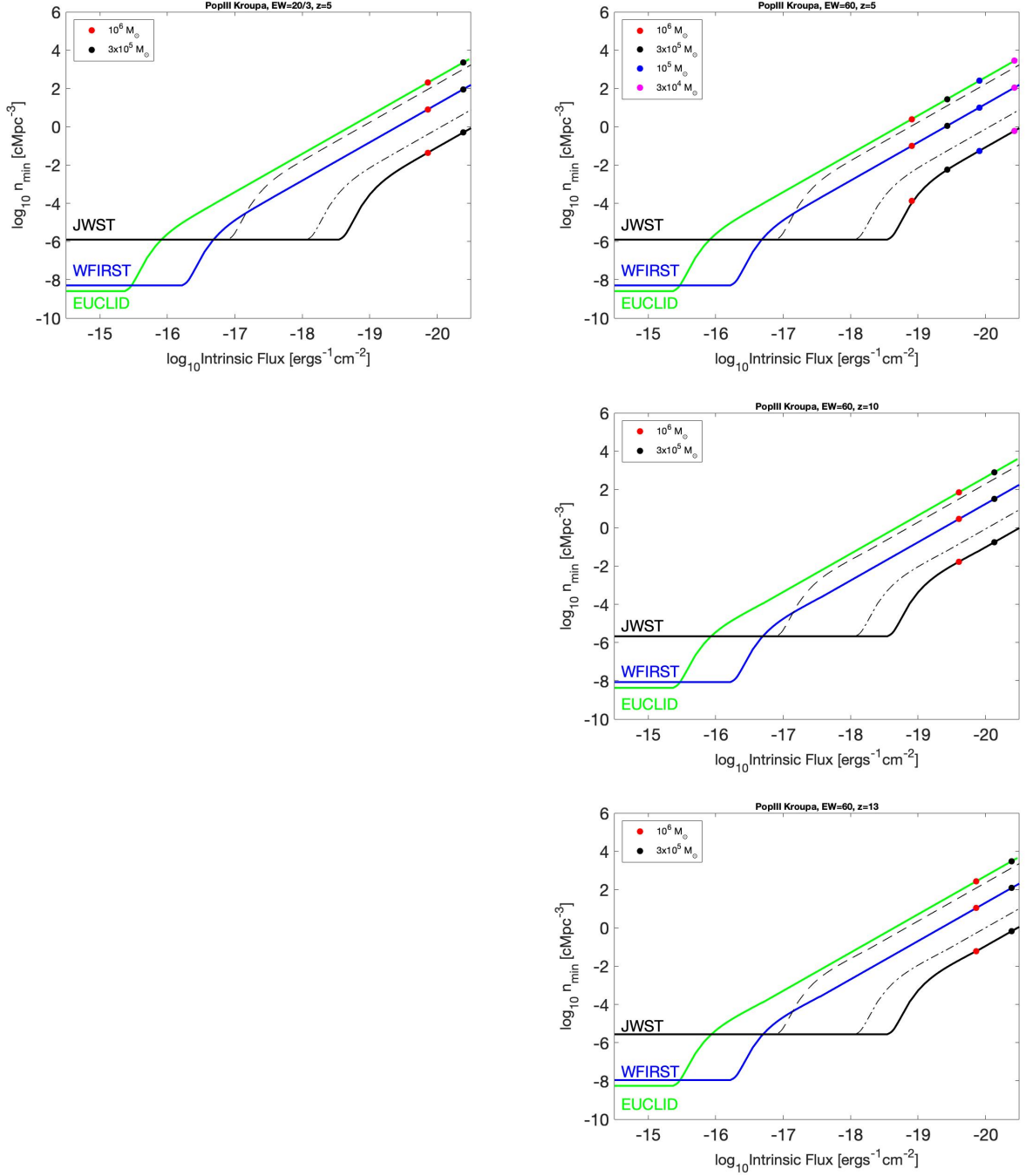


Figure 23: Comparing the spectroscopic detectability of JWST, WFIRST and Euclid for PopIII Kroupa model with an EW of 20/3 and 60 at redshifts of 5, 10 and 13. For the case of EW 20/3 and redshifts 10 and 13, galaxies of all masses are pushed beyond number densities of 10^4 cMpc^{-3} and are not included. The dashed and dot-dashed black lines corresponds to the lower detection limits of JWST from table 2. For all redshifts, JWST is the preferred instrument for both the lower (20/3) and higher (60) limit for the equivalent width.

7 Conclusions

Provided that the models regarding the formation and evolution of population III stars and galaxies are not too far from the truth, the possibility for detection does not appear impossible. The most optimistic results are obtained through the usage of the very bright PopIII.1 model that contains only very massive stars, a model that might not be the best representation of the real mass distribution. There are also some promising results from the PopIII.2 model, where the distribution peaks at lower masses compares to PopIII.1, but it still contains mostly very massive stars. Previously it was believed that PopIII.1 provided the best description of population III stars, but pushing the IMF towards less extreme masses might give a better image with the true population III IMF ending up between these two models. But it is also a question of how massive population III galaxies can get. The more massive, the more luminous, but exactly how massive a population III galaxy can get is still an open question, with the current results giving a maximum mass of roughly $2.5 * 10^6 M_{\odot}$ which theoretically puts the galaxies within the reach of the telescopes discussed here. This means that a non-detection result is in a way also useful since it provides information about upper limits on for example galaxy number densities or sets restrictions to the parameters used.

7.1 Future outlook

Since the telescope included here are not yet launched, they are what can be expected in the nearest future. Hopefully they will keep their latest schedule and soon be able to provide us with information and clues about the very first light of the universe.

References

- [A. Tanikawa et al. 2018] A. Tanikawa et al. 2019, Metal pollution of low-mass Population III stars through accretion
- [Ryan et al 2000] Ryan et al. 2000, Primordial lithium and big bang nucleosynthesis
- [L.Germany et al.] COSMOS - The SAO Encyclopedia of Astronomy, <http://astronomy.swin.edu.au/cosmos/-/-About>
- [P.H. Bodenheimer 2011] Peter H. Bodenheimer, 2011, Principles of Star Formation, ISBN 978-3-642-15062-3
- [V. Pirronello et al. 1998] V. Pirronello et al. 1998, Formation of molecular hydrogen: the mother of all molecules
- [J.L. Johnson 2011] Formation of the First Galaxies: Theory and Simulations Jarrett L. Johnson
- [E. Visbal et al. 2017] E. Visbal et al. 2017, What is the maximum mass of a Population III galaxy?
- [H. Yajima et al. 2016] H. Yajima 2016, upper limits on the mass and luminosity of Population III galaxies
- [M. Stiavelli & M. Trenti 2009] Stiavelli & Trenti 2009, Formation rates of Population III stars and chemical enrichment of halos during the reionization era
- [A.T.P. Schauer et al. 2019] A.T.P. Schauer et al. 2019, Constraining the first star formation with 21 cm cosmology
- [E. Zackrisson et al. 2012] E. Zackrisson et al. 2012 Detecting gravitationally lensed Population III galaxies with the Hubble Space Telescope and the James Webb Space Telescope
- [E. Zackrisson et al. 2011] E. Zackrisson et al. 2011, The spectral evolution of the first galaxies. I. JWST detection limits and colour criteria for Population III galaxies

- [C. Rydberg et al. 2012] C. Rydberg et al. 2012, Detection of isolated population III stars with the James Webb Space Telescope
- [A. Stacy et al. 2010] A. Stacy et al. 2010, The first stars: formation of binaries and small multiple systems
- [T. H. Greif et al. 2011] T. H. Greif et al. 2011, The delay of population III star formation by supersonic streaming velocities
- [K. Inayoshi et al. 2018] K. Inayoshi et al. 2018, Massive black hole and Population III galaxy formation in overmassive dark-matter haloes with violent merger histories.
- [M. Stiavelli & M. Trenti 2010] M. Stiavelli and M. Trenti 2010, The clustering properties of the first galaxies
- [A. Fialkov et al. 2012] A. Fialkov et. al 2012 “Impact of the relative motion between the dark matter and baryons on the first stars: semi-analytical modelling”
- [A. Raiter et al. 2010] A. Raiter et al. 2010 Predicted UV properties of very metal-poor starburst galaxies
- [P. Schneider 2009] P. Schneider 2009, “Cosmology” Lecture Notes, Argelander-Institut für Astronomie, Universität Bonn
- [R. S. Ellis 2009] Richard S. Ellis 2009, Gravitational lensing: a unique probe of dark matter and dark energy
- [Tejaswi Venumadhav et al. 2017] Tejaswi Venumadhav et al. 2017, Microlensing of Extremely Magnified Stars near Caustics of Galaxy Clusters
- [P. L. Kelly et al. 2018] Patrick L. Kelly et al. 2018, Extreme magnification of an individual star at redshift 1.5 by a galaxy-cluster lens
- [K. Kuijken 2003] Konrad Kuijken 2003, The basic of lensing

- [R. Goullioud et al. 2014] R. Goullioud et al. 2014, Wide Field Infrared Survey Telescope (WFIRST): Telescope design and simulated performance
- [J.P. Gardner et al. 2006] J.P. Gardner et al. 2006, The James Webb Space Telescope
- [R.J. Laureijs et al. 2010] R.J. Laureijs et al. 2010, The Euclid Mission